The SvFUL2 transcription factor is required for inflorescence determinacy and timely flowering in Setaria viridis

Jiani Yang , ¹ Edoardo Bertolini , ¹ Max Braud, ¹ Jesus Preciado, ^{2,‡} Adriana Chepote, ¹ Hui Jiang ¹ and Andrea L. Eveland ¹ I,*, [†]

- 1 Donald Danforth Plant Science Center, Saint Louis, Missouri, 63132, USA
- 2 National Science Foundation Research Experiences in Plant Science at the Danforth Center, Saint Louis, Missouri, 63132, USA

Research Article

J.Y. and A.L.E. designed and advised the research. J.Y., M.B., J.P., A.C., and H.J. performed genetics and morphological experiments. E.B. performed GRN analyses. M.B. performed gene editing. J.Y. and E.B. performed data analyses. J.Y., E.B., and A.L.E. wrote the paper. All authors have read and approved the manuscript for submission.

The author responsible for distribution of materials integral to the findings presented in this article in accordance with the policy described in the Instructions for Author (https://academic.oup.com/plphys/pages/general-instructions) is: Andrea L. Eveland (aeveland@danforthcenter.org)

Abstract

Inflorescence architecture in cereal crops directly impacts yield potential through regulation of seed number and harvesting ability. Extensive architectural diversity found in inflorescences of grass species is due to spatial and temporal activity and determinacy of meristems, which control the number and arrangement of branches and flowers, and underlie plasticity. Timing of the floral transition is also intimately associated with inflorescence development and architecture, yet little is known about the intersecting pathways and how they are rewired during development. Here, we show that a single mutation in a gene encoding an AP1/FUL-like MADS-box transcription factor significantly delays flowering time and disrupts multiple levels of meristem determinacy in panicles of the C₄ model panicoid grass, *Setaria viridis*. Previous reports of *AP1/FUL*-like genes in cereals have revealed extensive functional redundancy, and in panicoid grasses, no associated inflorescence phenotypes have been described. In *S. viridis*, perturbation of *SvFul2*, both through chemical mutagenesis and gene editing, converted a normally determinate inflorescence habit to an indeterminate one, and also repressed determinacy in axillary branch and floral meristems. Our analysis of gene networks connected to disruption of *SvFul2* identified regulatory hubs at the intersection of floral transition and inflorescence determinacy, providing insights into the optimization of cereal crop architecture.

Introduction

Inflorescence structure determines fruit, seed, and pollen production, which are critical for reproductive success of plants and global food security. During the shift from vegetative to reproductive growth, the indeterminate shoot

apical meristem (SAM), which patterns the vegetative organs, transitions to an inflorescence meristem (IM). Like the SAM, the IM continues indeterminate growth but instead, leaf growth is suppressed and axillary meristems (AMs) grow out into reproductive organs on its flanks. In

^{*}Author for communication: aeveland@danforthcenter.org

[†]Senior author.

[†]Present address: Plant Molecular and Cellular Biology Program, University of Florida, Gainesville, Florida, 32611, USA.

eudicot systems such as Arabidopsis (*Arabidopsis thaliana*), the IM directly lays down floral meristems (FMs), which produce flowers. In grasses, FMs are borne from spikelet meristems (SMs) either directly from the IM as in wheat (*Triticum aestivum*) and barley (*Hordeum vulgare*), or after a series of AM branching events such as in maize (*Zea mays*) and sorghum (*Sorghum bicolor*). Eventually, AMs acquire SM identity and terminate in a spikelet, the central unit of the grass inflorescence, housing one to several flowers that bear grain. Variation in activity and determinacy of AMs and SMs in grasses allows for the wide diversity of inflorescence branching patterns (*Tanaka* et al., 2013; Whipple, 2017; Bommert and Whipple, 2018).

Inflorescence architecture is also shaped by the activity and determinacy of the IM. In certain cereals such as rice (*Oryza sativa*), barley, and maize, the IM is indeterminate and continues meristematic activity, laying down lateral structures until it ceases growth. Alternatively, in wheat and sorghum, the IM takes on a determinate fate and produces a defined number of AMs before terminating in a spikelet. IM determinacy has been linked to flowering time through the action of multiple common regulators, which also affect branching patterns in the inflorescence (Danilevskaya et al., 2010; Li et al., 2019; Liu et al., 2019a). A weak flowering signal tends to delay meristem determinacy in the inflorescence, allowing for increased branch outgrowth and higher order branch initiation (McSteen et al., 2000; Endo-Higashi and Izawa, 2011; Boden et al., 2015).

Much of what we know about the molecular underpinnings of IM determinacy comes from Arabidopsis, which produces an indeterminate inflorescence. In Arabidopsis, indeterminacy in the IM is maintained by the antagonistic relationship between TERMINAL FLOWER 1 (TFL1) and floral identity genes, LEAFY (LFY), APETALA1 (AP1), and CAULIFLOWER (CAL; Piñeiro and Coupland, 1998; Liljegren et al., 1999; Serrano-Mislata et al., 2017). AP1 and CAL belong to the euAP1 subclade of the AP1/FUL (FRUITFUL)-like MADS box gene family and are key players in controlling flowering time and AM determinacy (Kempin et al., 1995; Alvarez-Buylla et al., 2006). TFL1, which encodes a phosphatidylethanolamine-binding protein, is expressed in the central region of the IM and prevents it from acquiring FM identity by suppressing floral identity genes (Weigel et al., 1992; Bradley et al., 1997; Benlloch et al., 2007). Loss of TFL1 function results in the mis-expression of AP1 and LFY in the IM, causing a terminal flower(s) to form in place of the indeterminate meristem, early flowering, and enhanced determinacy of lateral branches (Shannon and Meeks-Wagner, 1991; Alvarez et al., 1992). Alternatively, mutations in AP1 and LFY genes result in the production of indeterminate lateral shoots, which typically develop determinate FMs and have delayed flowering (Irish and Sussex, 1990; Schultz and Haughn, 1991; Huala and Sussex, 1992; Weigel et al., 1992; Bowman et al., 1993; Schultz and Haughn, 1993).

The regulatory modules that control inflorescence growth habit are somewhat conserved between eudicots and

grasses. In maize and rice, TFL1-like genes delay flowering time and prolong the indeterminate status of the developing inflorescence (Nakagawa et al., 2002; Danilevskaya et al., 2010; Kaneko-Suzuki et al., 2018). In rice, AP1/FUL-like genes have overlapping roles in flowering time (Kobayashi et al., 2012). Over-expression of OsMADS14, OsMADS15, or OsMADS18 all result in early flowering phenotypes (Jeon et al., 2000; Fornara et al., 2004; Lu et al., 2012), and in the case of OsMADS15, reduced panicle size and branch number (Lu et al., 2012). In winter wheat and barley varieties, expression of VERNALIZATION 1 (VRN1), an AP1/FUL-like gene, have been well-characterized as an early signal in promoting timely vegetative-to-reproductive transition in response to vernalization (Yan et al., 2003; Preston and Kellogg, 2008; Li et al., 2019). Expression of FUL2 and FUL3 genes in wheat are also induced by vernalization to promote flowering (Chen and Dubcovsky, 2012; Li et al., 2019). A recent study revealed that AP1/FUL-like genes in wheat and the genetic interactions among them contribute to maintenance of IM and SM determinacy, as well as flowering time (Li et al., 2019). Loss-of-function in both VRN1 and FUL2 genes converted the normally determinate IM of the wheat spike to an indeterminate habit, and also enhanced indeterminacy in primary AMs. Introduction of a single functional copy of either VRN1 or FUL2 reverted the vrn-null; ful1-null mutant IM back to a determinate habit (Li et al., 2019).

While evidence across the plant kingdom supports conserved roles for AP1/FUL-like genes in floral transition and inflorescence architecture, to date, there have been no inflorescence phenotypes described for loss-of-function AP1/FULlike genes in the subfamily Panicoideae, which includes agronomically important crops such as maize, sorghum, and sugarcane (Saccharum officinarum). This is likely due to functional redundancy (Litt and Irish, 2003; Preston and Kellogg, 2007). In this study, we show that a single loss-offunction mutation in an AP1/FUL-like gene in model panicoid grass, Setaria viridis (green foxtail), is sufficient to confer both strong flowering time and inflorescence determinacy phenotypes despite its overlapping expression pattern with three closely related paralogs. S. viridis is a weedy, C₄ species that has demonstrated promise as a model system for elucidating molecular mechanisms in panicoid crops (Li and Brutnell, 2011; Huang et al., 2017; Yang et al., 2018). It also represents a key evolutionary node between domesticated and undomesticated grasses. Like wheat, S. viridis produces a determinate inflorescence that terminates in a spikelet, but AMs undergo multiple orders of branching (Doust and Kellogg, 2002; Zhu et al., 2018). We isolated the Svful2 mutant in a genetic screen, which displayed a "barrel"-like panicle morphology due to enhanced indeterminacy in AMs. The determinate IM was also converted to an indeterminate habit resembling a maize ear. Further investigation of Svful2 loss-of-function at the molecular level using genomics approaches revealed regulatory modules that link floral transition and inflorescence determinacy pathways through interactions among MADS-box transcription factors (TFs) and several other developmental regulators. This mutant and the analyses presented here, provide insights into the complex interface of flowering time and inflorescence development, and potential targets for fine-tuning inflorescence ideotypes in cereal crops.

Results

Characterization of the barrel 1 mutant in S. viridis In a forward genetics screen of approximately 3,000 N-methylurea (NMU) mutagenized M2 families of S. viridis (Huang et al., 2017; Yang et al., 2018), we isolated the barrel1 (brl1) mutant, named for its abnormal, barrel-shaped panicle (brl1-ref allele). Compared with mature panicles of the wild-type mutagenized reference line (A10.1), mutant panicles were shorter and thicker and appeared more branchy (Figure 1, A and B; Table 1). Mutant plants were shorter in stature and produced tillers with more leaves (Figure 1A; Table 1). In addition to morphological defects, flowering time was obviously delayed in brl1 mutants. To test the effect of different photoperiods (Ppds) on floral transition,

we examined flowering time of the mutant compared to control plants under both short day (SD; 12-h light/12-h dark) and long day (LD; 16-h light/8-h dark) conditions. Under SD conditions, which typically promote flowering in S. *viridis* (Doust et al., 2017), *brl1* mutant panicles emerged ~6 d later (average 29.20 d after sowing [DAS]) than those of wild-type (average 22.94 DAS; Figure 1C). Under LD conditions, flowering time in *brl1* mutant (avg. 31.21 DAS) and A10.1 wild-type plants (average at 28.44 DAS) was delayed compared to under SDs, but *brl1* mutants still flowered significantly later than wild-type (average 3 d; Figure 1D; Table 1).

Previous studies in S. *viridis* showed that flowering time impacted both plant architecture and biomass (Doust, 2017). Under both LD and SD conditions, plant height and panicle length of *brl1* mutants were significantly shorter than wild-type plants at maturity (Table 1). Under SD conditions, above-ground dry weight was increased in mutants compared to wild-type, largely due to biomass of vegetative tissue (leaves and stems; Table 1). In LDs, above-ground dry weight of *brl1* mutants was comparable to wild-type,

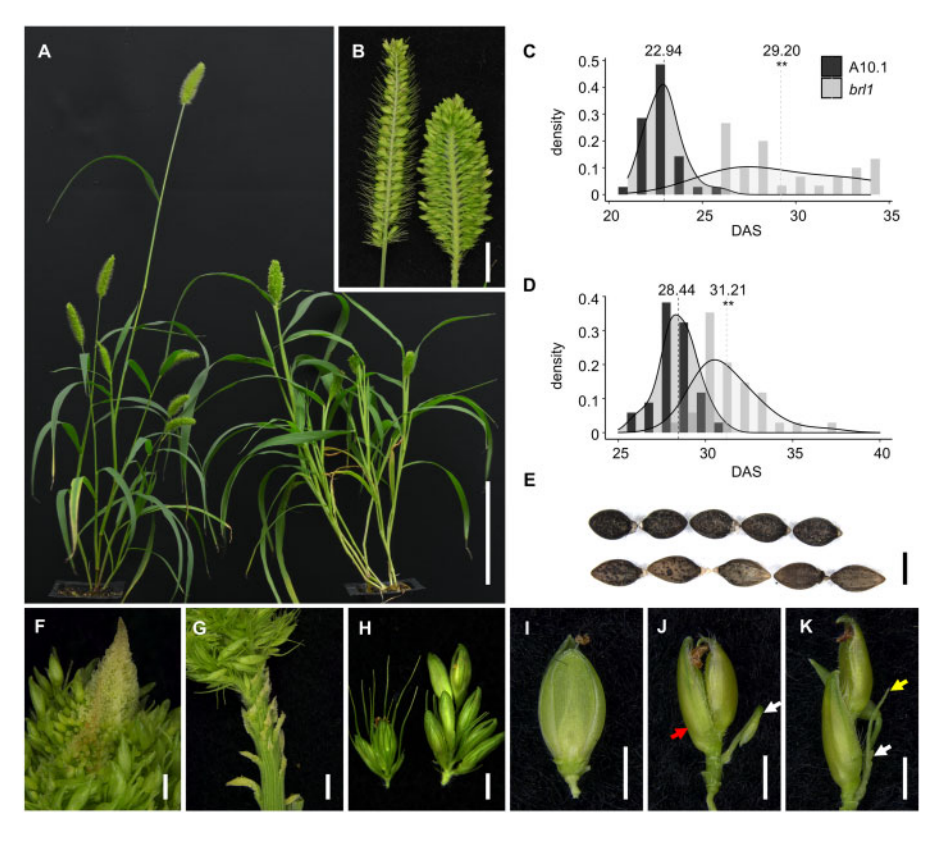


Figure 1 Characterization of the brl1 mutant phenotypes. A, Plant morphology of the wild-type A10.1 (left) and the brl1 mutant (right). Scale bar = 10 cm. B, Compared to the wild-type (left), brl1 mutant (right) panicles were shorter and wider, and primary branches were packed more densely. Primary branches were removed from one side of the panicle for a longitudinal view. Scale bar = 1 cm. Under SD (C) and LD (D) conditions, panicles of the brl1 mutant emerged significantly later than those of wild-type. **Student's t test P <0.01. E, Compared to wild-type (top), the brl1 mutant (bottom) produced longer and narrower seeds. Scale bar = 1 mm. F, In brl1 mutant panicles, the IM appeared indeterminant with continual production of primary branches. Scale bar = 1 mm. G, Rudimentary primary branches were visible at the base of mature panicles in the brl1 mutant. Scale bar = 1 mm. H, Primary branches in the brl1 mutant panicles (right) were markedly longer than those of A10.1 (left). Scale bar = 1 mm. Examples of phenotypes in brl1 mutant spikelets that lose SM maintenance (J and K), including aberrant development of the lower floret (red arrow, J) or production of additional bristles (yellow arrow, K) and spikelets (white arrow, J and K) within a spikelet, compared to A10.1 (l). Glumes were removed in l–K for better view. Scale bars = 1 mm.

Table 1 Phenotypic measurements of brl1 mutant plants compared to wild-type (A10.1) controls

Photoperiod	Trait	A10.1	brl1
LD	Days to panicle emergence (DAS)	28.44 ± 1.06	31.21 ± 1.82**
16-h Light/8-h Dark	Weight of leaves and stems (g)	3.83 ± 0.98	$4.73 \pm 0.65^{**}$
	Weight of panicles with seeds (g)	3.06 ± 1.14	$2.01 \pm 0.62^{**}$
	Plant height (cm)	61.72 ± 11.23	$35.81 \pm 3.75^{**}$
	Panicle length (cm)	6.25 ± 0.61	$5.03 \pm 0.71^{**}$
SD	Days to panicle emergence (DAS)	22.94 ± 0.97	$29.20 \pm 3.00^{**}$
12-h Light/12-h Dark	Weight of leaves and stems (g)	0.89 ± 0.25	$2.00 \pm 0.38^{**}$
	Weight of panicles with seeds (g)	1.45 ± 0.51	1.18 ± 0.53
	Plant height (cm)	30.95 ± 4.75	$16.74 \pm 2.00^{**}$
	Tiller No.	11.20 ± 3.93	$16.60 \pm 3.68^{**}$
	Leaf No.	38.00 ± 12.94	$126.25 \pm 29.97^{**}$
	Panicle length (cm)	3.53 ± 0.41	$3.16 \pm 0.50^{**}$
	Primary branch No.	36.55 ± 3.80	47.95 ± 9.56**
	Weight of 100 seeds (mg)	159.10	149.40
	Seed length (mm)	2.08 ± 0.06	$2.39 \pm 0.15^{**}$
	Seed width (mm)	1.28 ± 0.05	$1.21 \pm 0.07^{**}$
	IM ^a length (μm)	202.92 ± 23.55	$310.80 \pm 34.51^{**}$
	IM ^a width (μm)	65.50 ± 7.60	89.99 ± 10.45**

All data except for IM length and width (n > 9) are based on mean values of n > 20 individuals $(\pm so)$.

however, we still observed a significant increase in dry weight of vegetative tissue (leaves and stems) in the mutant (Table 1). Seed shape and size were also different with the mutant seeds being longer and narrower than those of wild-type (Figure 1E; Table 1).

Examination of the inflorescence morphology revealed that brl1 mutants displayed various levels of indeterminacy. At the tip of the panicle, the IM appeared indeterminate in mutants, and newly formed branch meristems (BMs) were still visible at maturity (Figure 1F). At the base of the mutant panicle, rudimentary primary branches were observed, which were not found in wild-type (Figure 1G). Primary branches were longer in brl1 mutants and the panicle rachis was clearly thicker (Figure 1H; Supplemental Figure S1A). Bristles, which are modified branches paired with spikelets in Setaria sp., did not elongate to the length of wild-type bristles, and so were largely found buried under spikelets (Figure 1H). In Setaria spp., spikelets form upper and lower FMs. During differentiation, the upper floret (uf) develops whorls of floral organs, that is, lemma and palea, lodicules, stamens, and pistil, within a pair of subtending glumes, and the lower floret is aborted. Development of spikelets and flowers was also affected in brl1 mutants, but phenotypes showed low penetrance with varied severities of indeterminacy. For example, \sim 17% of *brl1* mutant panicles produced additional flowers, bristles, and/or spikelets within spikelets compared to the typical one flower per spikelet in wild-type (Figure 1, I-K). The lemma and palea of mutant flowers were more elongated in the mutant and were more rigid, which is likely contributing to the elongated seed shape (Supplemental Figure S1, B and C).

brl1 mutants show loss of determinacy in various stages of inflorescence development

We used scanning electron microscopy (SEM, Figure 2) to compare the developmental progression of inflorescence

primordia from the brl1 mutant with that of wild-type S. viridis. By 11 DAS, the vegetative SAM of wild-type plants had finished transitioning to the reproductive IM, as the first primary BMs were initiated on its flanks (Figure 2A). In the brl1 mutant, the vegetative-to-reproductive transition was delayed to 15 DAS (Figure 2B), consistent with its late-flowering phenotype (Figure 1C). After the transition, wild-type inflorescences initiated primary branches in a spiral pattern (Figure 2C), and then secondary and tertiary axillary branches sequentially in a distichous pattern, as previously described (Figure 2E; Doust and Kellogg, 2002; Yang et al., 2018; Zhu et al., 2018). The brl1 IM was elongated compared to that of wild-type (Figure 2B and Table 1; Supplemental Figure S1, D and E), and this appeared to enable capacity for increased initiation of primary and higher-order branches (Figure 2, D and F), consistent with the mature panicle phenotype. By 17 DAS, the wild-type IM had become determinate and terminated as a spikelet (Figure 2G). BMs then began to differentiate from the tip of the inflorescence primordium into either an SM or a sterile bristle, and this continued basipetally (Figure 2, G and I). Conversely, the IM of the brl1 mutant remained indeterminate and continued to produce primary BMs at 21 DAS (Figure 2H), where SMs and bristles began to differentiate toward the top of the inflorescence primordium (Figure 2J). By the end of the developmental series analyzed by SEM, the brl1 IM remained indeterminate, which is consistent with its mature phenotype in Figure 1F.

While differentiation of SMs and bristles appeared normal in the mutant (Figure 2, I and J), the onset was delayed compared to wild-type and after additional rounds of higher-order branching (Figure 2F). SMs developed similarly in *brl1* mutants and wild-type, initiating glumes and upper and lower FMs; the uf typically develops into a perfect flower with lemma, palea, anther, and carpel and the lower

a Length and width of IM were measured at the end of the reproductive transition and before layout primary branches (Supplemental Figure S1, D and E).

^{**}Indicates a significant difference in brl1 mutant compared to A10.1 (wild-type) determined by Student's t test (P < 0.01).

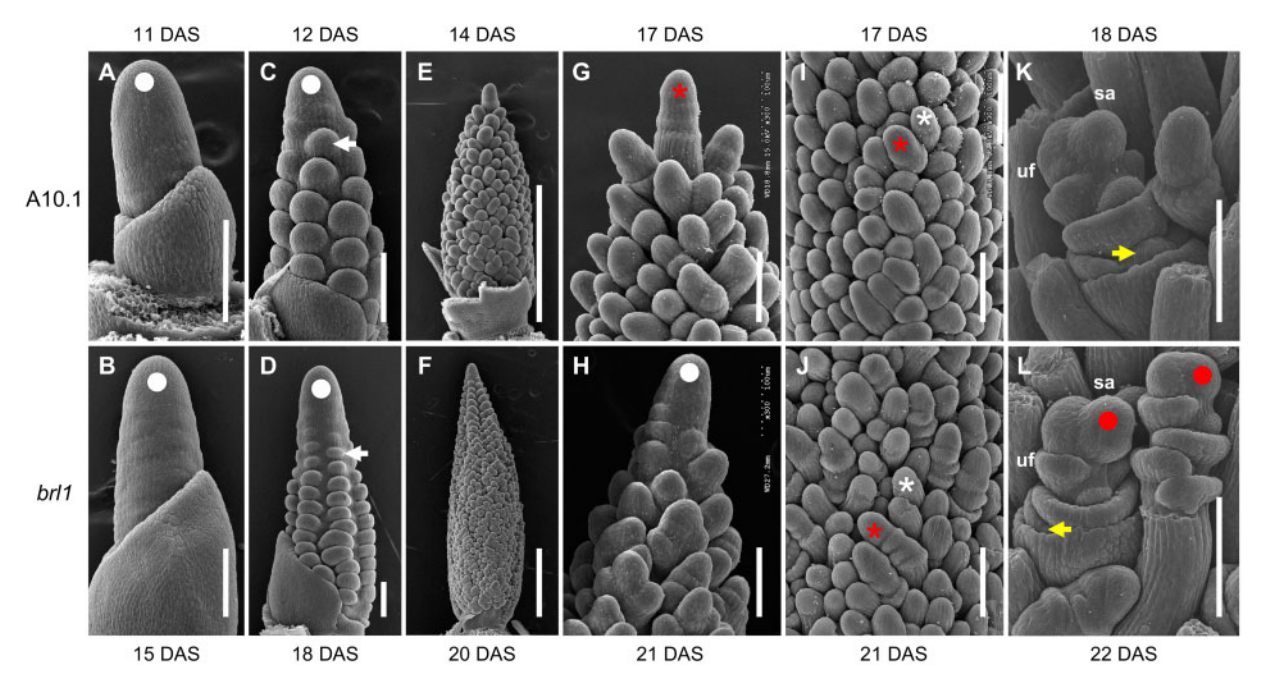


Figure 2 Morphological analysis of early inflorescence development in the *brl1* mutant by SEM. The transition from SAM to IM (IM = white dot) in the *brl1* mutant was delayed to 15 DAS (B) compared to 11 DAS in A10.1 (A). Branching capacities were increased in *brl1* panicles (D and F, 18 DAS and 20 DAS, respectively) compared to those of A10.1 (C and E, 12 DAS and 14 DAS, respectively). White dot indicates IM (not shown in E and F due to scale). White arrows indicate primary branches. In A10.1, the 17 DAS IM ceased to produce new BMs and terminated as the first SM (G, red asterisk) and then BMs started to differentiate into SMs (I, red asterisk) and bristles (I, white asterisk) basipetally. However, at 21 DAS, the *brl1* mutant IM continued initiating primary branches at the inflorescence tip (H, white dot), even after BMs acquired SM (J, red asterisk) or bristle identities (J, while asterisk). Some *brl1* spikelets had abnormal outgrowth of meristems (red dots) in ufs (L) compared to A10.1 spikelets (K). Yellow arrows indicate aborted lower florets. Scale bars = 100 μm in A–D and G–L. Scale bars = 500 μm in E and F. sa, spikelet axis.

floret aborts (Figure 2K; Doust and Kellogg, 2002; Yang et al., 2018). In some cases, we observed aberrant meristematic outgrowths in *brl1* FMs (Figure 2L) which may explain our observations of additional spikelets and bristles within some spikelets (Figure 1, I and J). Our SEM analysis showed that a determinacy program was delayed in the IM, BMs, and SMs of *brl1* mutants.

The brl1 locus encodes SvFUL2, a MIKC-type MADS-box TF

F2 populations were generated from a cross between the brl1 mutant and the parental line, A10.1. Wild-type and barrel-like panicle phenotypes segregated with the expected Mendelian 3:1 ratio (139:48; P [χ^2 , 1 d.f.] = 0.83), which indicated that brl1 is a single locus recessive allele. To map the brl1 locus, Bulk Segregant Analysis (BSA) was performed (Michelmore et al., 1991; Schneeberger, 2014) with a pool of DNA from 30 brl1 mutant individuals from the segregating F2 population that was sequenced to approximately $92\times$ coverage (244.2M reads). Reads were aligned to the A10.1 reference genome (phytozome.jgi.doe.gov; version 2.1; Mamidi et al., 2020) and single nucleotide polymorphisms (SNPs) were called using GATK. Three high-confidence, nonsynonymous SNPs were identified and supported by high observed allele frequency (Supplemental Figure Supplemental Data Set S1). One candidate SNP disrupted

the start codon of Sevir.2G006400, a MIKC-type MADS-box gene, and was supported by whole-genome sequencing of the brl1 mutant (Figure 3, A and B). Sevir.2G006400 had previously been annotated as SvFul2 based on phylogenetics and evolutionary developmental analyses (Preston et al., 2009; Zhu et al., 2018). The other two non-synonymous changes which generated missense mutations in Sevir. 2G174301 and Sevir.7G048300 on chromosomes 2 and 7, respectively, were not identified by whole-genome sequencing of the brl1 mutant, indicating that they might be randomly fixed mutations by selfing (Supplemental Data Set S1). Unlike our previous experience with mapping by BSA in this population (Yang et al., 2018), we did not resolve a clear peak in the genomic region surrounding SvFul2, likely due to its position at the end of chromosome 2 where recombination rates are relatively higher and break linkage.

We designed a dCAPs marker specific for this SNP and genotyped over 200 segregating F2 individuals. Our genotyping results showed that this SNP co-segregated with the barrel panicle phenotype at 100% (Supplemental Figure S3). Transcript levels of SvFul2 were strongly reduced in the mutant inflorescence primordia compared to wild-type early in development based on RT-PCR (Supplemental Figure S4).

SvFul2 encodes the ortholog of OsMADS15 in rice, an AP1/FUL-like MADS-box gene in the MIKC-type

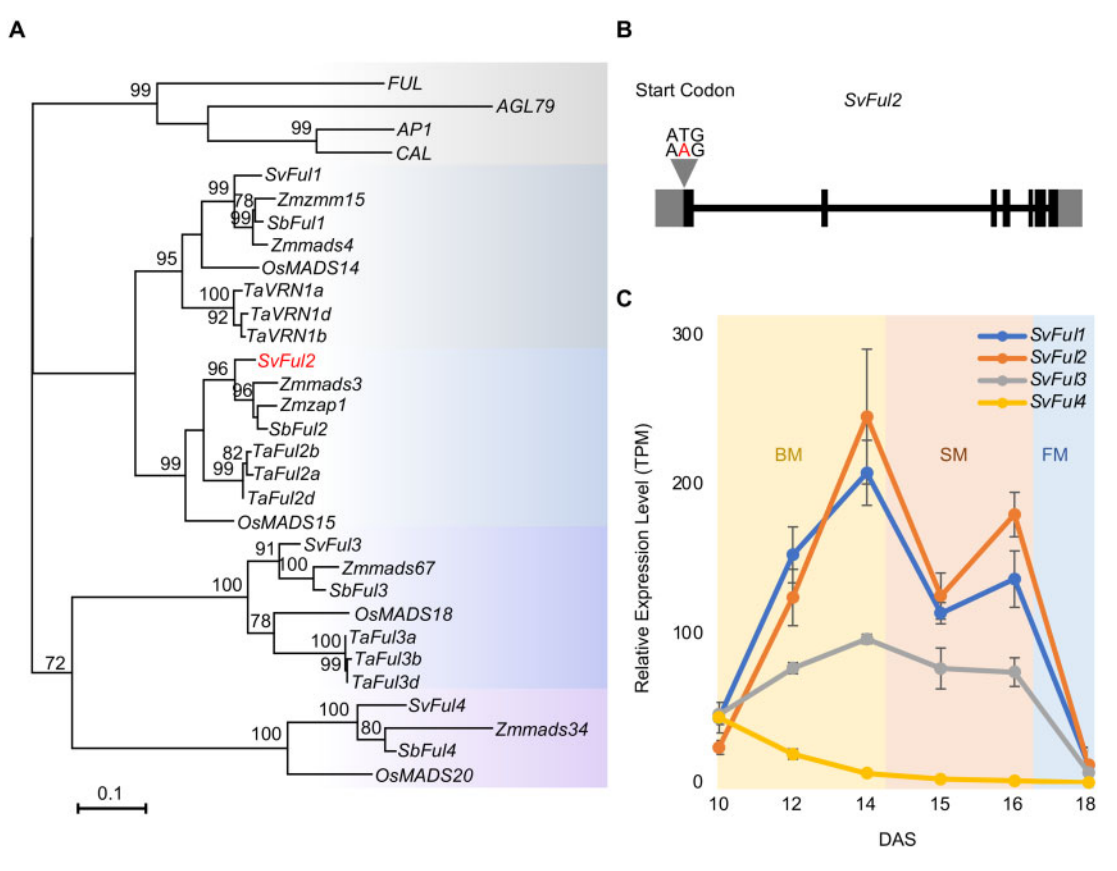
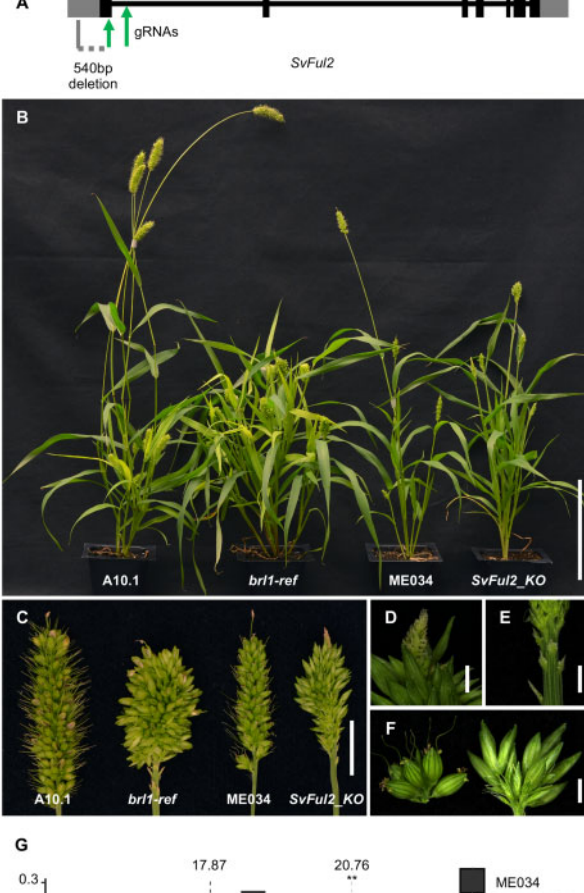


Figure 3 Phylogeny of AP1/FUL-like MADS-box genes in grasses and Arabidopsis and their expression profiles during S. *viridis* inflorescence development. A, Phylogenetic analysis of AP1/FUL-like MADS-box genes from S. *viridis*, Arabidopsis, and several grass species based on protein coding sequence. SvFul2 is highlighted in red. Os = Oryza sativa, Ta = Triticum aestivum, Zm = Zea mays, Sb = Sorghum bicolor, Sv = Setaria viridis. B, Exon-intron structure of the SvFul2 gene consists of seven exons (solid rectangles) and six introns (horizontal line). The S'- and S'-untranslated regions are shown as gray rectangles. Gray triangle indicates the location of the SNP that disrupts the start codon within the SvFul2 gene. C, Expression profiles (RNA-seq) of four S. *viridis* AP1/FUL-like MADS-box genes across six stages of early inflorescence development based on the transcriptomics resource described in (Zhu et al., 2018). Error bars indicate standard errors of three to four biological replicates.

subfamily. Consistent with previous phylogenetic studies (Wu et al., 2017; Li et al., 2019), our phylogenetic analysis of AP1/FUL-like MADS-box genes from S. viridis as well as Arabidopsis, rice, wheat, maize, and sorghum showed that SvFul2 was located in the FUL2 subclade along with three copies of wheat Ful2s, rice OsMADS15, and maize zap1 and mads3 (Figure 3A; Supplemental Data Set S2). SvFul2 is more closely related to SvFul1 (Sevir.9G087300) in the FUL1 subclade, which includes wheat VRN1s, rice OsMADS14, maize zmm15, and zmmads4. SvFul3 (Sevir.2G393300) and SvFul4 (Sevir.3G374401) are located in the FUL3 and FUL4 subclades, respectively. By examining a previously generated transcriptomics resource across six sequential stages of early S. viridis inflorescence development (Zhu et al., 2018), we found that SvFul1, SvFul2, and SvFul3 shared similar spatiotemporal expression patterns, increasing during branching and then decreasing during floral development with a small drop during spikelet specification (Figure 3C). SvFul1 was expressed highest at 10 and 12 DAS and SvFul2 expressed more at later stages, which indicate the two may have different functions. Comparatively, *SvFul4* was expressed at lower levels throughout inflorescence development, its expression gradually decreasing after the reproductive transition.

Gene editing of SvFul2 validates the mutant phenotype in S. viridis

To validate that Sevir.2G006400 (*SvFul2*) is responsible for the observed phenotypes of the *brl1* mutant, we used genome editing. A clustered regularly interspaced short palindromic repeats (CRISPR)/Cas9 construct was designed containing two guide (g)RNAs that specifically targeted the first exon and the first intron of *SvFul2*, respectively, in the highly transformable *S. viridis* accession, ME034 (Figure 4A; Acharya et al., 2017; Van Eck, 2018). In the T1 generation, individual plants carrying a homozygous 540-bp deletion in the first exon of *SvFul2* were selected (Figure 4A; Supplemental Figure S5). We called this genotype *SvFul2_KO*. These were moved forward to generation T2 where they were then outcrossed to ME034 and then selfed to select Cas9-free *SvFul2_KO* plants for phenotyping. *SvFul2_KO* plants displayed phenotypes consistent with



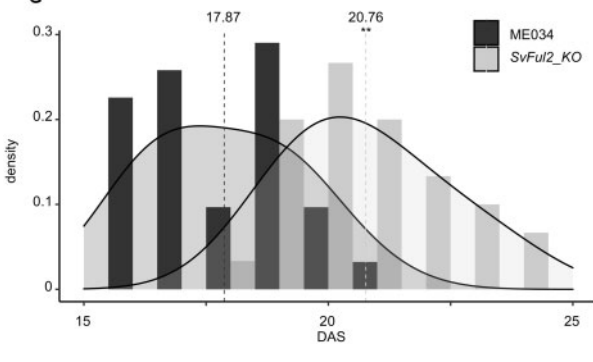


Figure 4 CRISPR/Cas9-based gene editing of SvFul2 phenocopied the brl1 mutant. A, Schematic diagram of the SvFul2 gene model showing locations of the two guide (g)RNAs target sites (green arrows) and the 540-bp deletion region (gray dashed line) in $SvFul2_KO$ plants. Plant morphology (B) and inflorescence structure (C) of the $SvFul2_KO$ mutant phenocopied that of the brl1 mutant. From left to right: A10.1, brl1-ref, ME034, and $SvFul2_KO$ individuals. Scale bars = 10 cm and 1 cm in A and B, respectively. Indeterminate IM (D), underdeveloped primary branches at the panicle base (E), and longer primary branches (F, right) were also observed in $SvFul2_KO$ panicles. Scale bars = 1 mm. G, Under SD conditions, panicle emergence day of $SvFul2_KO$ is significantly delayed compared to ME034. **Student's t test t < 0.01.

those of the *brl1* mutant (Figure 4, B–G). Compared with ME034 normal plants, *SvFul2_KOs* were shorter and branchy with more leaves (Figure 4B; Supplemental Table S1), and panicles displayed increased densities of longer primary branches (Figure 4, C and F; Supplemental Table S1). As

observed in *brl1* mutants, panicles of *SvFul2_KOs* took on an indeterminate growth habit (Figure 4D). Flowering time was also delayed in the *SvFul2_KOs* (avg. 20.76 DAS) compared to the ME034 wild-type siblings (avg. 17.87 DAS) by ~3 d (Figure 4G; Supplemental Table S1). The ME034 accession flowers earlier than A10.1, consistent with the shift in flowering time shown here. SEM analysis of *SvFul2_KO* during early inflorescence development showed floral transition consistent with the ME034 panicle emergence data, and increased branching capacity and IM indeterminacy as observed in *brl1-ref* (Supplemental Figure S6).

We further tested the allelic relationship between *brl1-ref* and *SvFul2_KO* by a genetic cross. *brl1-ref* and *SvFul2_KO* fail to complement and are allelic (Figure 5). Taken together, our analyses support *SvFul2*, Sevir. 2G006400, as the locus responsible for the *brl1* mutant phenotypes in *S. viridis*.

Loss of SvFul2 function alters expression of flowering and meristem determinacy pathways

To determine the molecular mechanisms underlying the complex phenotypes of the Svful2 mutant, we used RNAseq to profile gene expression in mutant inflorescence primordia across three key developmental transitions and compared them to equivalent stages in wild-type controls: right before (Stage 1) and after (Stage 2) the floral transition, and during the initiation of spikelet specification (Stage 3; Supplemental Figure S7; Supplemental Data Set S3). Here, we expect to capture transcriptional changes related to both differences in flowering time and meristem determinacy. For each stage, we profiled four biological replicates, each consisting of pooled, hand-dissected inflorescence primordia. Differential expression was determined using DESeq2 (1.22.2). Our analysis found 382, 2,584, and 2,035 differentially expressed genes (DEGs) at Stages 1-3, respectively (Supplemental Data Set S4). Based on Principal Component Analysis (PCA), we observed fewer differences in the mutant transcriptome at Stage 1, suggesting that the main influence of SvFul2 on inflorescence development begins once the SAM has initiated transition to the IM (Figure 6A). We also observed dynamic shifts in DEGs among the three stages; only 33 DE genes were shared across all three stages, and 149, 451, and 68 were shared between Stages 1 and 2, Stages 2 and 3, and Stages 1 and 3, respectively (Figure 6B). This suggests that SvFul2 potentially modulates different target genes in various spatiotemporal contexts. Indeed, indirect effects due to differences in cell populations, especially at Stage 3 after phenotypes of Svful2 and wild-type inflorescences have diverged, likely underlie a portion of stagespecific DEGs.

As expected, the SvFul2 gene itself was significantly down-regulated in mutant inflorescences at all three stages (Figure 6C). The other three S. viridis AP1/FUL-like genes were significantly upregulated in the mutant, suggesting that



Figure 5 Allelism test between *brl1-ref* and *SvFul2_KO* fail to complement the mutant phenotype. A cross between the *brl1-ref* mutant (A10.1 background) and *SvFul2_KO* (ME034 background) resulted in a bi-allelic F1 that showed an indeterminate panicle phenotype. F1 plants from a cross between A10.1 and *SvFul2_KO* showed normal-looking panicles. From left to right: panicles from *brl1-ref/SvFul2_KO* F1, A10.1/*SvFul2_KO* F1, *brl1-ref*, A10.1, *SvFul2_KO*, and ME034. Scale bar = 2 cm.

the four AP1/FUL-like genes may provide some level of functional compensation during inflorescence development. Two B-class genes, SvMads16 (AP3) and SvMads4 (PISTILLATA), which in grasses are typically expressed at low levels prior to floral organ development (Whipple et al., 2004), were upregulated in Svful2 Stage 2 inflorescences (Figure 6C). In addition, two E-class genes were differentially expressed in mutant inflorescences: SvMads34 was upregulated at Stages 1 and 2, while SvMads5 was downregulated at Stage 2 (Figure 6C). In rice, OsMADS34 coordinates with AP1/ FUL-like genes, and physically interacts with some of them, to specify IM identity (Kobayashi et al., 2012). In general, E-class genes play partially redundant roles in specifying floral organ identities via protein-protein interactions with other MADS box proteins (Pelaz et al., 2000; Honma and Goto, 2001; Theißen and Saedler, 2001; Ditta et al., 2004).

Since the transition to reproductive growth is delayed in Svful2 mutants, we expected to see changes in genes and pathways associated with flowering time (Figure 6D). Functional categories related to flowering time were overrepresented among DEGs post-transition at Stage 2, including "vegetative to reproductive phase transition of meristem" (GO:0010228; P adj = $3.75e^{-02}$) and "vernalization response" (GO:0010048; P adj = 3.68e⁻⁰²; Figure 6E; Supplemental Data Sets S5 and S6). Homologs of well-characterized genes known to regulate flowering in other species were differentially expressed (Figure 6D). For example, the putative S. viridis orthologs of rice OsFTL1 (Sevir.5G151301, SvFtl1) encoding florigen (FT protein) and OsFD1 (Sevir.2G302300, SvFd1), were upregulated at Stage 2. In Arabidopsis, FD is repressed by AP1 (Kaufmann et al., 2010). In addition, members of FLC-like and TM3/SOC1-like MIKC-type MADS-box genes and CONSTANS-like genes, which are also implicated in floral transition (Zhang et al., 2015; Huang et al., 2018), were among DEGs upregulated in Svful2 mutants at Stage 2 (Figure 6, C and D). Putative S. viridis orthologs of zea mays

centroradialis (zcn) genes encoding FT homologs were differentially expressed. For example, SvZcn2 (Sevir.1G183200), which is phylogenetically closest to Arabidopsis TFL1 (Danilevskaya et al., 2008, 2010), was upregulated in Svful2 mutants at all three stages. In Arabidopsis, AP1 and TFL1 act antagonistically to repress each other's expression to modulate flowering time and IM determinacy (Shannon and Meeks-Wagner, 1991; Alvarez et al., 1992; Kaufmann et al., 2010).

Consistent with defects in meristem determinacy, DEGs in Svful2 mutants were enriched for functions related to meristem development with overrepresented gene ontology (GO) terms such as "meristem initiation" (GO:0010014; p.adj = $7.63e^{-04}$) and "stem cell development" (GO:0048864; P.adj = 0.0046; Figure 6E; Supplemental Data Set S6). Upregulated DEGs included homologs of AP2-like genes in maize known to suppress indeterminate growth in the SM, including indeterminate spikelet1 (Sevir.9G034800) and sister of indeterminate spikelet1 (SvSid1, Sevir.2G093800; Supplemental Figure S8; Chuck et al., 1998, 2007, 2008). The homolog of rice MOTHER OF FT AND TFL1 (Sevir.4G169200, SvMtf1), which represses SM identity, was also upregulated in Svful2, and the ortholog of maize ramosa2 (SvRa2; Sevir.5G116100), which functions to promote meristem determinacy (Bortiri et al., 2006), was downregulated (Supplemental Figure S8).

As a consequence of increased meristem indeterminacy, Svful2 mutant inflorescences branch more. We also found that genes associated with "anatomical structure formation involved in morphogenesis" (GO:0048646) were overrepresented among DEGs at stages 1 (P.adj = 0.0027) and 2 ($P.adj = 3.65e^{-08}$; Figure 6E; Supplemental Data Set S6), consistent with enhanced expression of genes involved in organogenesis. Among this functional class were putative orthologs of known genes that specify abaxial cell fate, for example, Sevir.1G255800 (SvYab15) and milkweed pod1 (Sevir.6G158800; Candela et al., 2008), and adaxial cell fate,

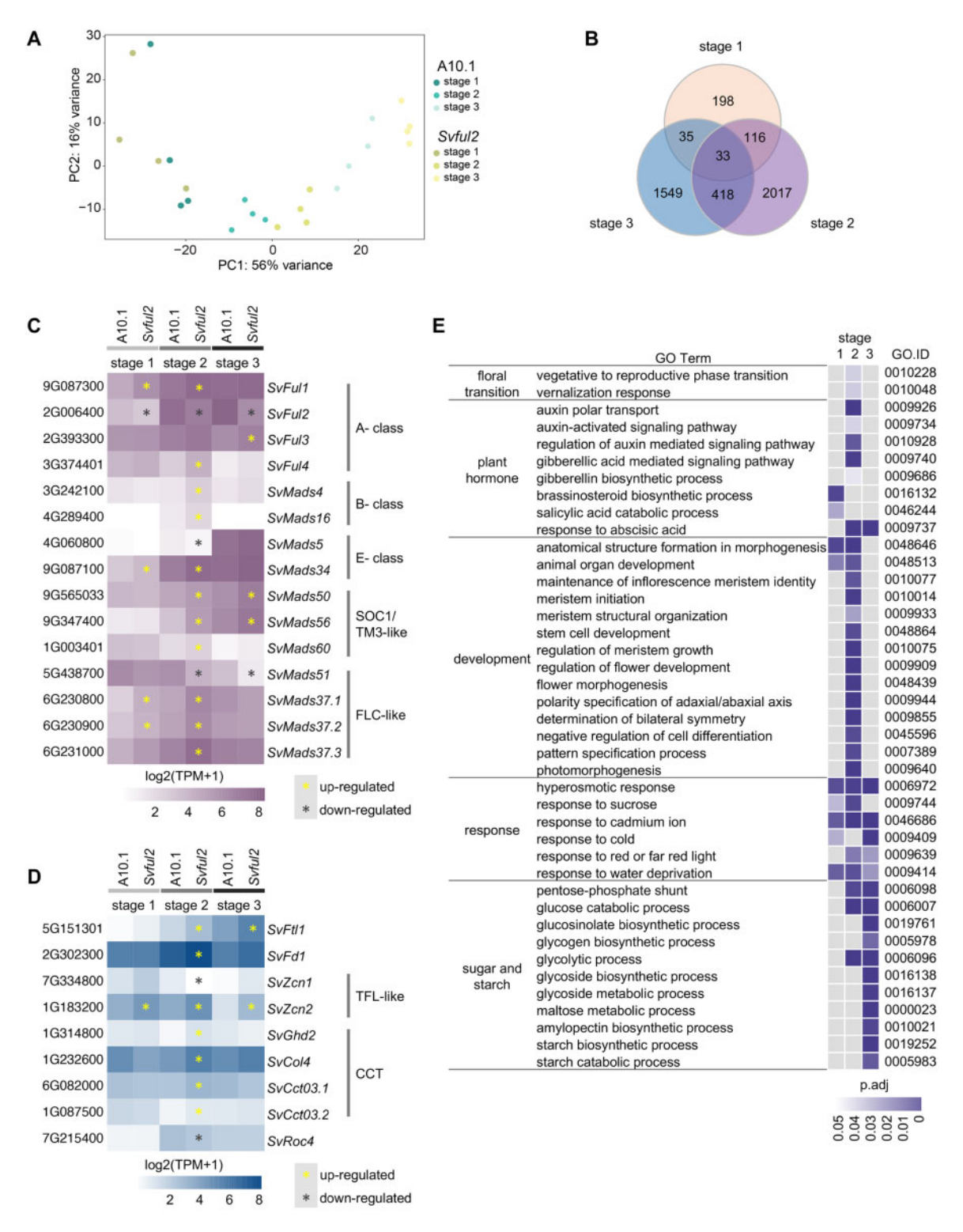


Figure 6 Transcriptional changes in Svful2 mutants across three stages of inflorescence development. A PCA showed that biological replicates were well-correlated with each other and that PC1 (explaining 56% of the variance) was associated with developmental stage. Loss-of-function in Svful2 resulted in fewer transcriptional changes prior to the floral transition with larger changes between genotypes appearing later in development. B, DEGs showed dynamic transcriptional changes across three stages of inflorescence development in Svful2 mutants. Among DEGs were several encoding MADS-box TFs (C) and known regulators of flowering time (D). TPM values were Log2 transformed to generate heatmaps. Yellow and black asterisks indicate up and downregulated DEGs (FDR < 0.05), respectively. E, Subsets of GO terms that were overrepresented among DEGs at each of the three developmental stages. P adj <0.05.

for example. Rice outermost cell-specific gene5 (Sevir.5G077800) and **PHABULOSA** (Sevir.9G157300); McConnell et al., 2001; Juarez et al., 2004; Zou et al., 2011), which were upregulated in the mutant (Supplemental Figure S8). Alternatively, the putative ortholog of rice DWARF3, SvD3 (Sevir.4G068300), which functions in suppression of branching through the strigolactone signaling pathway (Zhou et al., 2013), was downregulated (Supplemental Figure S8). The major transcriptome changes observed in loss-of-function mutants at Stage 2 reflect a core function for SvFUL2 in modulating the reproductive transition at the molecular level, but also how it links delayed flowering to suppression of meristem determinacy programs.

Transcriptional rewiring by perturbation of SvFul2 reveals sub-networks connecting reproductive transition and determinacy pathways

To further investigate how SvFul2 connects within a larger gene network to regulate flowering time and meristem determinacy pathways, we used a computational strategy based on weighted gene co-expression network analysis (WGCNA) and a random forest classifier to construct a gene regulatory network (GRN) representing normal inflorescence development in S. viridis (A10.1). Here, we integrated RNA-seq data from a previous study that captured precise stages of A10.1 inflorescence primordia spanning the IM transition to the development of floral organs (Zhu et al., 2018) with the staged wild-type data collected in this study. Using the WGCNA algorithm (Langfelder and Horvath, 2008), we clustered 26,758 genes into 27 co-expression modules (Figure 7A; Supplemental Figure S9 and Supplemental Data Set S7). Module eigengenes (MEs; expression pattern that best fits an individual module) were evaluated for their significant associations with four key developmental events represented in the network: the vegetative-to-reproductive transition (8 and 10 DAS), branching (11, 12, and 14 DAS), meristem determinacy (15-17 DAS), and flower development (18 DAS; Figure 7A). Within each module, we tested for enrichment of genes that were differentially expressed in the Svful2 mutant, and found several that showed enrichment during key developmental events (Figure 7A). Among these, MEmagenta showed a strong positive correlation with the floral transition and a negative correlation with meristem determinacy (Figure 7, A and B). MEmagenta showed enrichment for DEGs in Stages 1 and 2 (Figure 7A). Network analysis of this module revealed SvMads51 (Sevir.5G438700), which is orthologous to mads69 from maize, was predicted as a hub node in control of many genes, including the regulator of meristem determinacy SvSid1 (Liang et al., 2019; Supplemental Figure S10). In maize, mads69 has been associated with both floral transition and meristem determinacy. It is located in the maize QTL Vgt3 associated with flowering time and latitudinal variation, and it was recently validated as the transcriptional regulator of FT genes. ZmMADS69 was also associated with tassel branch number and tassel branch length (Liang et al., 2019). Alternatively, MEbrown showed a positive correlation with meristem determinacy, but was negatively correlated with the floral transition (Figure 7, A and B). SvFul2 and SvFul3 were both co-expressed in the brown module, along with 428 DEGs largely at Stages 2 and 3.

We also integrated the co-expression network with information derived from regulatory interactions among TFs and their putative targets based on the GENIE3 algorithm (Huynh-Thu et al., 2010). This complementary approach helped us to infer the directionality and connectivity of important hub genes within the gene network, yielding a directed graph of regulatory interactions. Based on the assumption that expression of a given gene is a function of the expression of the other genes in the network, we applied a regression trees method using as inputs TFs expressed in our dataset (n = 1,295) selected based on PlantTFDB (Jin et al., 2017), their expression trajectories in the network and those of other genes, to identify potential TF targets (Huynh-Thu et al., 2010). Regulatory genes and their predicted targets were restricted based on information from differential expression analysis between wild-type and the Svful2 mutant. We used the resulting regulatory framework to explore functional relationships between SvFUL2, its predicted direct targets, and predicted upstream regulators, particularly in the context of connecting floral transition and meristem determinacy. For example, magenta and brown modules were connected through a bHLH TF (Sevir.2G248500) that was predicted to directly target both SvMADS51 and SvFUL2 (Liang et al., 2019), placing it as a potential regulator at the intersect of flowering time and meristem determinacy (Supplemental Figure S11).

Our GRN also predicted that SvFUL2 controls several co-expressed TFs previously implicated in developmental processes, and localized to modules that positively associated with branching/meristem determinacy and negatively associated with floral transition (Figure 7C). Among these were SvRA2, and an INDETERMINATE DOMAIN TF, several members of which have been involved in both the floral transition and determinacy, including the founding member from maize, indeterminate 1 (id1; Colasanti et al., 1998; Kozaki et al., 2004). Our analyses point to a possible feedback loop mechanism between SvFUL2 and SvRA2, where SvFul2 is also a predicted direct target of SvRA2. We also observed putative feedback regulation between SvFUL2 and TFs encoded by putative orthologs of maize knotted 1 (kn1; TALE TF, Sevir.9G107600) and fasciated ear 4 (fea4; bZIP TF, Sevir.4G119100), which promote meristem maintenance and differentiation, respectively (Bolduc et al., 2012; Pautler et al., 2015). Extensive feedback among these developmental TFs could represent endogenous mechanisms for fine-tuning development during the floral transition and patterning of the inflorescence.

Discussion

According to the classic ABCDE model of floral development in Arabidopsis, A-class AP1/FUL-like MADS-box genes

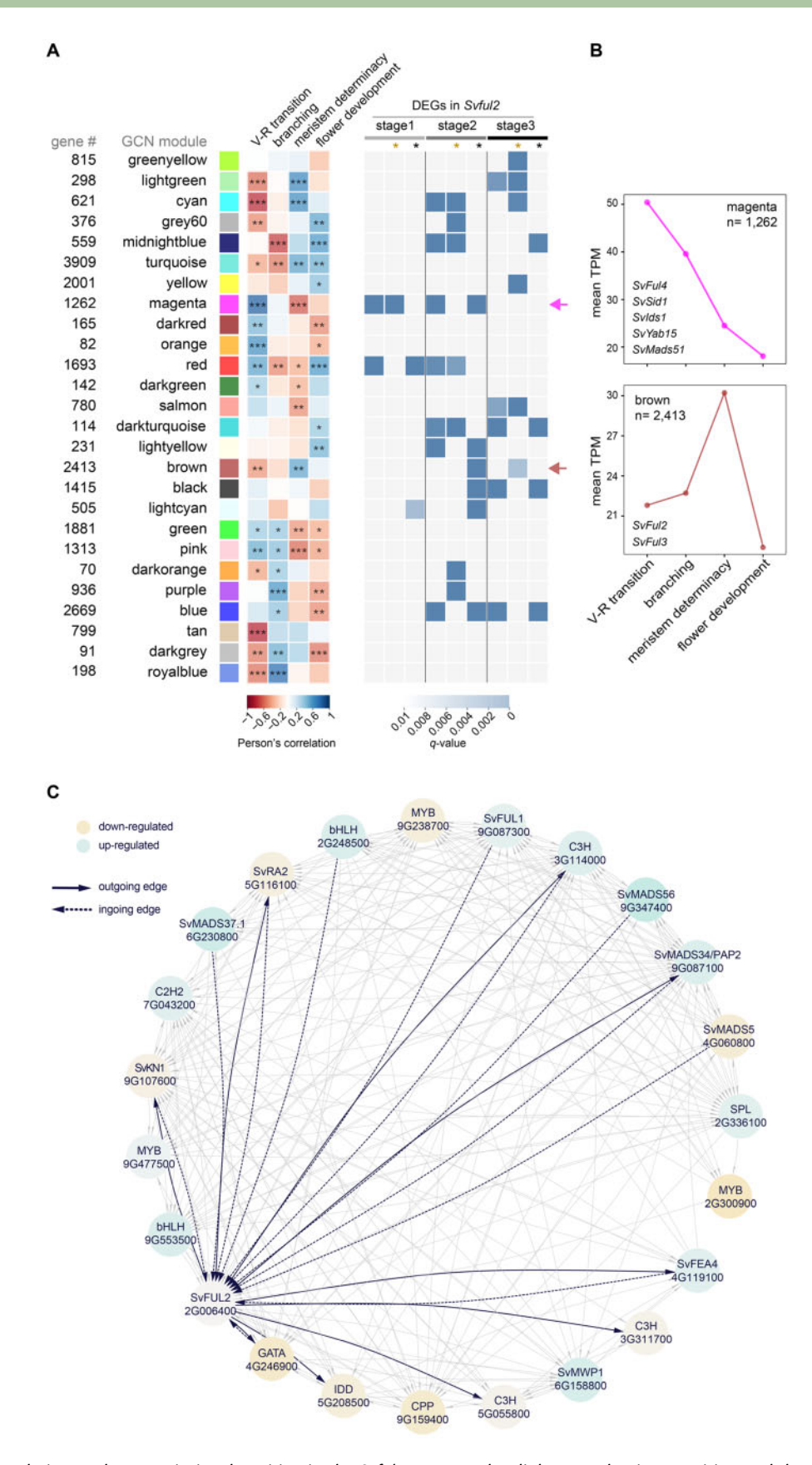


Figure 7 Network analysis reveals transcriptional rewiring in the Svful2 mutants that links reproductive transition and determinacy pathways. A, (left) Heatmap represents the WGCNA ME association with key events during early inflorescence development (vegetative-to-reproductive transition, branching, meristem determinacy, and flower development) in S. viridis. Network modules are represented and named with different colors based on the WCGNA default module annotation. Number of genes co-expressed in each module is indicated to the left. Student asymptotic P

have essential functions in modulating the floral transition and floral organ development (Irish and Sussex, 1990; Ferrándiz et al., 2000; Kaufmann et al., 2010). The roles of A-class genes have been the focus of extensive evolution and development studies (Litt and Irish, 2003; Preston and Kellogg, 2007); however, relatively little is known about their functions in grasses. Given the complex branching patterns that arise post-floral transition and prior to flower development in grasses, it is expected that there would be some variation in function. In general, grasses show subtle variations on the traditional ABCDE model, however, the underlying mechanisms are generally conserved (Ambrose et al., 2000; Whipple et al., 2007). Functional redundancy among A-class genes is widespread in grasses, and only recently have simultaneous perturbations in multiple paralogs revealed informative mutant phenotypes, for example, in rice and wheat (Wu et al., 2017; Li et al., 2019). So far there have been no inflorescence phenotypes reported for AP1/ FUL-like genes in any panicoid species, which include major cereal and energy crops. Therefore, we know little about their specific functions in regulating important agronomic traits such as flowering time and inflorescence determinacy. In this study using S. viridis as a model, we characterized a loss-of-function mutant in an AP1/FUL-like gene, SvFul2, that displayed strong developmental phenotypes, which was unexpected for a single mutant allele. Our morphological and molecular analyses of the Svful2 mutant provide insights into the roles of AP1/FUL-like genes in connecting flowering time and inflorescence determinacy in panicoid grasses, as well as predictions on conserved and novel regulatory interactions underlying the complex phenotypes.

SvFul2 is necessary for proper timing of flowering and determinacy programs

Phylogenetic studies have reconstructed the evolutionary history of AP1/FUL-like genes in angiosperms (Litt and Irish, 2003; Preston and Kellogg, 2006; Soltis et al., 2007; Wu et al., 2017). The monocot AP1/FUL-like clade members evolved independently after the split of monocots and eudicots (Litt and Irish, 2003; Preston and Kellogg, 2007). In the Poaceae clade, four copies of AP1/FUL-like genes are derived from three duplication events in the AP1/FUL lineage. The first likely occurred during early monocot evolution, giving rise to the FUL3 clade. The second occurred near the base of the Poaceae, which generated the FUL1 and FUL2 clades (Preston and Kellogg, 2006). The last duplication produced the FUL3 and FUL4 clades, and FUL4 was lost in some grass species during evolution (Wu et al., 2017). Such duplication events can lead to functional redundancy and subsequent Figure 7 (continued)

diversification. In grasses, AP1/FUL-like genes are expressed much earlier than in eudicots (Preston and Kellogg, 2007), and their transcripts have been detected in IM, BMs, and SMs in addition to floral organs. In several grass species studied, FUL1/VRN1/OsMADS14 and FUL2/OsMADS15 have redundant and/or overlapping spatiotemporal expression patterns in these three meristem types, yet show different patterns within the spikelet. This suggests that in certain grasses, these two genes play redundant roles during the floral transition and in SM identity, but diversified roles in floral organ identity.

Among the grasses, AP1/FUL-like genes have been most studied at the functional level in rice and wheat (Wu et al., 2017; Li et al., 2019), where clear functions in flowering time have been demonstrated. The role of SvFul2 in controlling flowering time is consistent with the significant accumulation of SvFul2 transcripts (over 100-fold change in expression in the IM) during the transition from SAM to IM (Figure 6C). SvFul1 and SvFul3 were also induced during this time (Figure 6C), but fold changes were not as large as for SvFul2, similar to what has been shown in rice (Kobayashi et al., 2012). Based on our results and previous studies, the accumulation of AP1/FUL-like transcripts in the IM upon the induction of FT is likely required for promoting the reproductive transition, and this is a conserved mechanism in grasses.

The shift from a determinate to indeterminate fate in the IM of Svful2 mutants (Figures 1F and 2H), which was also observed in the wheat vrn1-null; ful2-null double mutant, is reminiscent of the tfl1 mutant phenotype in Arabidopsis (Shannon and Meeks-Wagner, 1991). Previous studies that spatiotemporal expression of FUL1/VRN1/ OsMADS14 and FUL2/OsMADS15 in phylogenetically disparate grasses, showed that they are most abundantly expressed in the tip of the IM (Preston and Kellogg, 2007). In both Svful2 and wheat vrn1-null; ful2-null mutants, significant increases in the expression of TFL1 homologs were detected (Figure 6D; Li et al., 2019). These results suggest that the mechanism for controlling IM determinacy in grasses involves an antagonism between AP1/FUL-like genes and TFL1-like genes, as in eudicots. IM determinacy appears to be very sensitive to the activity of AP1/FUL-like genes. In wheat, complete loss of both VRN1 and FUL2 function leads to an indeterminate IM, while a single functional copy of VRN1 or FUL2 in a heterozygous state was able to recover a determinate IM. It has been proposed that indeterminate growth in the IM was derived from a determinate habit in evolution, which involved the modification and/or loss of an early common TFL1 mechanism (Bradley et al., 1997). This hypothesis could explain this apparent sensitivity.

for the ME association are indicated: ***P <0.001; **P <0.01, and *P <0.05. (right) Heatmap represents enrichment of Svful2 DEGs at each of the three developmental stages profiled in the mutant among the MEs. Gold and black asterisks indicate up- and downregulated genes, respectively, in the Svful2 mutant compared to wild-type. B, Expression trajectories of MEmagenta and MEbrown across S. viridis inflorescence development. Y-axis represents the average TPM of co-expressed genes in each module. C, Subnetwork of predicted direct targets of SvFUL2 and its direct up-stream regulators based on our GRN. Genes are represented as circles with edges linking specific regulators to their targets. Differential fold change of expression in the Svful2 mutant background is represented by the colored scale. Darker colors represent higher |fold change|.

The strong phenotypes we observed in S. viridis by a single knockout of an AP1/FUL-like gene indicate its central role in controlling multiple developmental processes. Interestingly, the co-expression of closely related paralogs, SvFul1 and SvFul3, with SvFul2 does not seem to provide much functional compensation, but we did see both genes upregulated upon SvFul2 perturbation (Figure 6C). SvFul2 was expressed at high levels (highest among other AP1/FUL-like genes) at most of the developmental stages we examined (Figure 3B). The localized expression of SvFul2 mRNAs was previously analyzed by in situ hybridization in a study by (Preston and Kellogg, 2007) to evaluate developmental expression patterns of AP1/Ful-like genes in inflorescence primordia across grasses. They showed that SvFul2 transcripts accumulated largely in the IM during early inflorescence development, consistent with its role in floral transition and determinacy. In addition, transcripts were detected in BMs and SMs, also consistent with indeterminacy in these meristem types in the loss-of-function Svful2 mutant. Expression patterns of SvFul1 and SvFul2 overlapped in these meristems but interestingly, diverged in developing FMs (Preston and Kellogg, 2007). SvFul2 showed distinct expression in marking floral organ primordia of the first two whorls, however, in our analyses of the Svful2 mutant, development of these organs appeared unaffected. This suggests that other factors potentially compensate for loss of SvFul2 in proper floral organ development in S. viridis.

The functional redundancy of AP1/FUL-like genes in grasses provides an opportunity for diversification of function, and a toolkit for fine-tuning development of desired traits.

SvFul2 as an integrator of flowering time and inflorescence determinacy

Connections between flowering time signals and meristem determinacy pathways in the inflorescence have been highlighted in various grass species. A strong flowering signal can impose meristem determinacy when perceived by the developing inflorescence (Dixon et al., 2018). For example, wheat Ppd-1, which functions in a Ppd-dependent floral induction pathway, suppresses paired spikelet formation through modulation of FLOWERING LOCUS T (Boden et al., 2015). The paired spikelet phenotype is associated with enhanced indeterminacy. In maize, loss-of-function in id1, a key player in the floral transition, leads to complete loss of meristem determinacy; instead of floral organs, plantlets are developed from every spikelet in mutant tassels (Colasanti et al., 1998). Meristem identity genes, for example, AP1/FULlike genes, have been proposed to function downstream of the flowering signal to promote meristem determinacy and reshape inflorescence architecture (Dixon et al., 2018).

In our study, the important role of *SvFul2* in coordinating flowing time and meristem determinacy is not only supported by its strong pleiotropic phenotypes, but also reflected in our predictions of regulatory relationships between *SvFUL2* and its upstream modulators and downstream targets. Several MADS-box TFs, most of which are

homologs to those implicated in flowering time, were predicted to directly target SvFul2 (Figure 7C). We also identified a bHLH TF of unknown function predicted to target both SvFul2 and SvMads51, which is the syntenic ortholog of the maize flowering time regulator mads69, and therefore a potential integrator of floral transition and meristem determinacy (Supplemental Figure S11). Interestingly, several other MADS-box TFs were shown to directly target SvFul2 based on predictions in our GRN: SvMADS37.1 (Sevir. 6G230800), SvMADS56 (Sevir.9G347400), SvMADS5 (Sevir. 4G060800), SvMADS34/PAP2 (Sevir.9G087100), and SvFUL1 (Figure 7C). SvMads34/Pap2 was also predicted to be a direct target of SvFUL2. These predictions are consistent with previous studies showing regulatory interactions among MADS-box TFs during the floral transition and inflorescence development. In rice, OsMADS37 and OsMADS56 have been functionally characterized as flowering time regulators. OsMADS34/PAP2 has been shown to function redundantly with rice AP1/FUL-like genes to promote flowering and SM determinacy (Kobayashi et al., 2010, 2012), and OsMADS5 is involved in spikelet identity (Wu et al., 2018). Our analysis indicates that SvFUL2 may function as a core integrator at the interface of these closely linked developmental programs through feedback coordination with several other developmental TFs.

Our network analysis also uncovered potential feedback regulation between SvFUL2 and SvRA2 (Figure 7C), which could point to a conserved mechanism by which flowering links to AM determinacy in grasses. SvRa2 is the ortholog of maize ra2 and barley Six-rowed spike4 (Vrs4; Bortiri et al., 2006; Koppolu et al., 2013). Both ra2 and Vrs4 function in imposing determinacy on spikelet pair meristems and triple SMs in maize and barley, respectively. Although several downstream targets of ra2 and Vrs4 have been identified through genetic and/or transcriptomics analyses (Bortiri et al., 2006; Bai et al., 2012; Koppolu et al., 2013; Eveland et al., 2014), upstream regulators have not been described. Unlike other genes in the RAMOSA pathway, ra2 function is highly conserved across grasses and expresses early during AM initiation, and temporally after the expression of AP1/ FUL-like genes (Bortiri et al., 2006; Koppolu et al., 2013; Zhu et al., 2018). In addition, localization studies have shown that ra2 and Ful2 are expressed in overlapping domains within BMs during early inflorescence development (Bortiri et al., 2006; Preston and Kellogg, 2007; Koppolu et al., 2013). The conserved spatiotemporal expression pattern of ra2 is consistent with it being downstream of FUL2 to potentially coordinate the flowering signal with regulation of meristem determinacy. Further functional studies are required to determine the genetic and molecular interactions between RA2 and FUL2.

In maize, over-expression of the maize AP1/FUL-like gene, zmm28, enhanced grain yield potential through improved photosynthetic capacity and nitrogen utilization (Wu et al., 2019). Direct targets of ZMM28 revealed through integrated RNA- and ChIP-seq analyses included genes involved in

photosynthesis and carbohydrate metabolism. Homologs of several of these targets were differentially expressed in Svful2 mutants, including photosystem I light-harvesting complex gene 6 (Sevir.2G22720), a gene encoding a pyruvate orthophosphate dikinase (Sevir.3G253900), and gene encoding a bZIP TF (Sevir.3G396500). Although SvFul2 encodes a different AP1/FUL-like gene in a different spatiotemporal context, we also observed changes in genes associated with photosynthesis and with sugar and starch metabolism in Stage 3 inflorescences where the mutant was highly indeterminate compared to wild-type. There could be common regulatory interactions between AP1/FUL-like genes associated with photosynthesis, carbon allocation, and sugar signals that link flowering time cues from the leaf to inflorescence architecture. We know little about the mechanisms by which sugar signals interface with development, but clear links, for example with trehalose-6-phosphate, underlie flowering time (Wahl et al., 2013), and meristem determinacy (Satoh-Nagasawa et al., 2006).

The striking phenotype displayed in loss-of-function Svful2 mutants enables us to more clearly define molecular connections between flowering time and various aspects of IM determinacy. One question that comes to mind is why do the pathways regulated by SvFul2 in S. viridis have fewer checks and balances in terms of functional redundancy compared to other grasses? Since S. viridis is an undomesticated weed, one hypothesis is that selection against indeterminacy phenotypes in inflorescences of modern cereal crop species masks the ability to recover individual functions of A-class genes at the phenotypic level. Furthermore, perhaps the phenotypes presented in Svful2 mutants provide plasticity in S. viridis's adaptability to a wide range of environmental conditions. In any case, our analyses of this mutant provide a glimpse into AP1/FUL-like gene function in panicoid grasses and predict regulatory interactions linking key yield traits that can be translated to important cereal and energy crops.

Methods

Plant materials and growth conditions

The *brl1-ref* mutant allele was isolated from an NMU mutagenized M2 population of S. *viridis* (Huang et al., 2017). The mutant allele was backcrossed to the reference mutagenized line (A10.1) and selfed to generate F2 segregating populations. F4 seeds were used for phenotyping, SEM, and RNA-seq experiments. *Setaria viridis* plants for phenotyping were grown under either SD (12-h light/12-h dark) or LD (16-h light/8-h dark) conditions (31°C/22°C [day/night], 50% relative humidity, and light intensity of 400 µmol/m²/s) in a controlled high-light growth chamber at the Danforth Center's growth facility. *Setaria viridis* plants used for SEM and RNA-seq were grown under the SD conditions.

SEM analysis

For SEM analysis, brl1 mutant and wild-type inflorescence primordia were harvested from young seedlings to examine

the developmental defects of mutants. Samples were fixed, hand-dissected, and dehydrated as described (Hodge and Kellogg, 2016). The dehydrated samples were critical point dried using a Tousimis Samdri-780a and imaged by a Hitachi S2600 SEM at Washington University's Central Institute of the Deaf.

Histology

Wild-type and mutant inflorescence primordia were harvested right after the vegetative-to-reproductive transition at 11 and 15 DAS, respectively. The samples were fixed, embedded, and sectioned as described by (Yang et al., 2018). Sections (10 μ m) made with a Microm HM 355S microtome (ThermoFisher, Waltham, MA, USA) were deparaffinized, stained with eosin, and imaged with a ZEISS AxioZoom microscope.

Bulked segregant analysis

M3 mutant individuals were crossed to the A10.1 reference line and resulting F1 individuals were self-pollinated to generate segregating F2 families. The F2 individuals with mutant and wild-type phenotypes were identified, and the segregation ratio was tested by a χ^2 test. DNA extracted from 30 brl1 mutant individuals was pooled to generate a DNA library. The DNA library was made using the NEBNext Ultra DNA Library Prep Kit for Illumina (NEB), size selected for inserts of 500-600 bp, and sequenced with 150-bp pairedend using standard Illumina protocols on Illumina Hi-Seq 4000 platform at Novogene. DNA libraries for whole-genome sequencing were generated from a single brl1 mutant individual in the M2 generation and sequencing with 100-bp single end on Illumina Hi-Seq 2,500 platform at University of Illinois, Urbana-Champaign W.M. Keck sequencing facility. Read mapping and SNP calling by GATK (3.5-0-version 3.5-0-g36282) were performed as described (Huang et al., 2017).

Phylogenetic analysis

The coding sequences of Arabidopsis, S. *viridis*, maize, sorghum, rice, and wheat *AP1/FUL-like* family genes were obtained from Phytozome (phytozome. jgi.doe.gov; Supplemental Data Set S2) and aligned using ClustalW to build a maximum likelihood tree with bootstrapping (1,000 iterations) in MEGA7 (Kumar et al., 2016).

CRISPR/Cas9 gene-editing

The genome sequence of *SvFul2* (Sevir.2G006400) was obtained from the *S. viridis* version 2.1 genome (https://phy tozome.jgi.doe.gov/). CRISPR-P version 2.0 (Liu et al., 2017) was used to design guide (g)RNAs to minimize off-targets. Two gRNAs targeting *SvFul2* were designed at the first exon and the first intron, 133- and 395-bp downstream of the ATG start codon, respectively. Using a plant genome engineering toolkit (Čermák et al., 2017), gRNAs were combined into a level 0 construct followed by insertion into a plant transformation vector. PCR amplified fragments from pMOD_B_2303 were merged using golden-gate cloning with T7 ligase and Sapl/BsmBl restriction enzymes back into the

pMOD B 2303 backbone to express the two gRNAa from the CmYLCV promoter, each flanked by a tRNA. This construct, along with pMOD_A1110 (a wheat codon-optimized Cas9 driven by the ZmUbi1 promoter) and pMOD_C_0000 modules, were combined in a subsequent golden-gate cloning reaction with T4 ligase and Aarl restriction enzyme into the pTRANS 250d plant transformation backbone. The final construct was cloned into Agrobacterium tumefaciens line AGL1 for callus transformation of S. viridis ME034 at the DDPSC Tissue Culture facility. To plantlets were genotyped for the presence of the selectable marker, hygromycin phosphotransferase to validate transgenic individuals. In the T1 generation, individual plants with possible mutant phenotypes were selected and the region of the target sites was amplified using PCR and sequenced. A homozygous 540-bp deletion in the first exon of SvFul2 was identified. These T1 mutants were self-pollinated to obtain T2 progeny and outcrossed to ME034 and then selfed to select Cas9free SvFul2 KO plants. Primer sequences used for vector construction and genotyping are listed in Supplemental Table S2.

RNA-seq library construction, sequencing, and analysis

Poly-A⁺ RNA-seq libraries were generated from pools of hand-dissected inflorescence primordia from wild-type and *Svful2* mutant seedlings. Wild-type primordia were sampled at 8, 11, and 17 DAS while, accounting for the mutant's developmental progression, *Svful2* primordia were sampled at 9, 15, and 21 DAS. For each developmental stage, four biological replicates were collected, for a total of 24 data points.

RNA was extracted (PicoPure RNA isolation kit; Thermo Fisher Scientific) and subjected to library preparation from 500 ng of total RNA using the NEBNext Ultra Directional RNA Library Prep Kit (Illumina, San Diego, CA, USA), size-selected for 200-bp inserts, and quantified on an Agilent bioanalyzer using a DNA 1,000 chip. RNA-seq libraries were processed using an Illumina HiSeq 4000 platform at Novogene with a 150-bp paired-end sequencing design. On average, for each data point ~20 million cleaned reads were generated. RNA-seq reads were quality checked and processed using the wrapper tool Trim Galore (version 0.4.4_dev) with the parameters "-length 100 -trim-n illumine." Cleaned reads were mapped to the S. viridis transcriptome (Sviridis_500_version 2.1; Phytozome version 12.1, phytozome.jgi.doe.gov) using Salmon (0.13.0) with the parameters "-validateMappings -numBootstraps 30," based on an index generated by primary transcripts (n = 38,209). Gene normalized expression levels (transcript per kilobase million [TPM]; Supplemental Data Set S3) and the count matrix for downstream analyses were determined from Salmon output files and imported in R using the Bioconductor package tximport (Soneson et al., 2015).

Sample variance was computed based on PCA with the function *dist* and *plotPCA* on variance stabilizing

transformation (vst) scaled data. Analyses of differential expression were performed using the Bioconductor package *DESeq2* (version 1.22.2) with default parameters for the Wald test. The Benjamini–Hochberg method for multiple testing correction was used to classify DEGs passing the *P*-value adjusted cut-off of 0.05.

For GO enrichment analysis, we generated a refined *S. viridis* GO annotation (Supplemental Data Set S5) using the GOMAP pipeline (https://gomap-singularity.readthedocs.io; Wimalanathan and Lawrence-Dill, 2019) to determine overrepresentation of GO terms within gene sets with the Bioconductor package *topGO*. GO testing was performed based on the Fisher's exact test method.

DE genes enriched in GCN modules were obtained based on the enrichment analysis using the function *enricher* from the Bioconductor package *clusterProfiler* (Yu et al., 2012) Benjamini–Hochberg multiple test corrections.

Weighted gene co-expression network analysis

In addition to the samples described above, we included previously described wild-type S. viridis inflorescence primordia samples (Zhu et al., 2018): 23 additional data points from 6 inflorescence stages (10, 12, 14, 15, 16, and 18 DAS). This dataset (GSE118673) was re-processed using the same methods described above and used to build a reference wild-type gene co-expression network spanning S. viridis inflorescence organogenesis, from the transition to reproductive phase to flower development. To reduce samples bias, we first filtered out genes with less than 10 counts (row sum <10), then we calculated the Euclidean distance and Pearson's correlation among samples and removed all replicates with rho coefficient < 0.92 or with a Euclidean score <0.8. Based on this, two samples were removed (8 DAS rep 4 and 17 DAS rep 3). Read counts from genes (n = 26,758) and samples (n = 33) passing the above filters were normalized with vst using the function vst from the Bioconductor package DESeq2.

A signed co-expression network was built using the blockwiseModules function from the WGCNA R package (Langfelder and Horvath, 2008) with the parameters: "power = 16, corType = "bicor", minModuleSize = 30, mergeCutHeight = 0.25, maxBlockSize = 30,000, MaxPoutlier = 0.05, minModuleSize = 20." The topological overlap matrix was calculated from the blockwiseModules function using the parameter "TOMType = 'signed.""

The module-to-developmental stage association was conducted evaluating the significance correlation of the ME and four key developmental stages defined as: (1) vegetative-to-reproductive transition (8 and 10 DAS); (2) branching (11, 12, and 14 DAS); (3) meristem determinacy (15–17 DAS); and (4) flower development (18 DAS). To conduct this analysis, we created a metafile where all samples were classified according to the four key stages. The R function *cor* and *corPvalueStudent* were used to test the correlation between ME and the stages. *Rho* values were used to identify relationship between modules and developmental stages.

Modules with $\it rho > |0.8|$ were considered strongly correlated to the developmental stages.

To predict targets of *S. viridis* TFs we built a complementary network using a machine learning approach with the Bioconductor package GENIE3 (Huynh-Thu et al., 2010). *Setaria viridis* TFs were downloaded from PlantTFDB (http://planttfdb.gao-lab.org; Jin et al., 2017) and overlapped with the expression matrix used in the WGCNA analysis to identify the expressed TFs in our dataset (n = 1,265). These TFs were used as probes to predict regulatory links between the putative targets and their expression trajectories in our dataset. We ran GENIE3 with the parameters "treeMethod = "RF", nTrees = 1,000" and putative target genes were selected with a weight cutoff ≥ 0.005 . Networks were explored and plotted using the R package *iGraph*.

Data accessibility

All sequence data, including whole-genome sequence data, raw and processed RNA-seq data, and associated metadata have been deposited in the NCBI Gene Expression Omnibus under accession number GSE156047.

Accession numbers

GenBank accession numbers for *S. viridis AP1/FUL-like* genes are as follows: *SvFul1* (XM_034716904; Sevir.9G087300), *SvFul2* (XM_034727736; Sevir.2G006400), *SvFul3* (XM_034726136; Sevir.2G393300), and *SvFul4* (XM_004962888; Sevir.3G374400). A more complete list of accession numbers for *AP1/FUL-like* genes discussed in this manuscript can be found in *Supplemental Data Set S2*.

Supplemental data

The following supplemental materials are available in the online version of this article.

Supplemental Figure S1. Additional characteristics of the *brl1* mutants (supports Figure 1).

Supplemental Figure S2. BSA analysis of the *brl1* locus.

Supplemental Figure S3. Genotyping of brl1 F₂ seedlings using a designed dCAPS marker for the SNP located at the start codon of SvFul2.

Supplemental Figure S4. RT-PCR results showing the reduced *SvFul2* expression level in mutant inflorescence primordia compared with A10.1.

Supplemental Figure S5. PCR genotyping of the SvFul2_KO CRISPR edited line.

Supplemental Figure S6. Morphological analysis of early inflorescence development in SvFul2_KO by SEM.

Supplemental Figure S7. Three key developmental transitions of *brl1* mutant and wild-type inflorescence development captured by RNA-seq profiling gene expression.

Supplemental Figure S8. Dynamic expression differences of genes related to meristem maintenance, plastochron, abaxial/adaxial cell fate, and meristem determinacy between wild-type and *Svful*2 mutant.

Supplemental Figure S9. Dendrogram representing relatedness among genes based on expression across all samples and their respective module assignments (indicated by color classification).

Supplemental Figure \$10. Gene co-expression subnetwork of the magenta module showing the relationship among key transcriptional regulators and hub genes.

Supplemental Figure S11. Gene regulatory sub-network showing predicted targets of SvMADS51 and its direct upstream regulators.

Supplemental Table S1. Phenotypic measurements of *SvFul2-KO* plants

Supplemental Table S2. Table of primers used in this study

Supplemental Data Set S1. High-confidence SNP calls for the *brl1* mutants.

Supplemental Data Set S2. Alignment of coding sequences of *AP1/FUL-like* genes by ClustalW.

Supplemental Data Set S3. Transcript abundances (TPM) for all annotated S. *viridis* genes (version 2) in the wild-type compared with Svful2 mutant inflorescence primordia.

Supplemental Data Set S4. DEGs with annotation at three developmental stages determined by DESeq2.

Supplemental Data Set S5. GOMAP for S. viridis.

Supplemental Data Set S6. Overrepresentation of functional classes among DEGs based on GO term enrichment.

Supplemental Data Set S7. Weighted gene co-expression network generated with the R package WGCNA (available at GEO: GSE156047).

Acknowledgments

The authors would like to thank Kevin Reilly and his team at the Integrated Plant Growth Facility (Danforth Center) for chamber maintenance and plant care and Veena Veena and her team at the Tissue Culture Facility (Danforth Center) for *S. viridis* transformation.

Funding

This work was funded by the National Science Foundation Plant Genome Research Program award #IOS_1733606 to A.L.E. and the Donald Danforth Plant Science Center. JP was funded by National Science Foundation REU Site grant: Research Experiences in Plant Science at the Danforth Center (NSF-DBI-REU-1156581). H.J. was funded by Department of Energy Biological and Environmental Research award #DE-SC0008769.

Conflict of interest statement: None declared.

References

Acharya BR, Roy CS, Estelle AB, Vijayakumar A, Zhu C, Hovis L, Pandey S (2017) Optimization of phenotyping assays for the model monocot Setaria viridis. Front Plant Sci 8: 2172

Alvarez-Buylla ER, García-Ponce B, Garay-Arroyo A (2006) Unique and redundant functional domains of APETALA1 and

- CAULIFLOWER, two recently duplicated *Arabidopsis thaliana* floral MADS-box genes. J Exp Bot **57**: 3099–3107
- Alvarez J, Guli CL, Yu XH, Smyth DR (1992) terminal flower: a gene affecting inflorescence development in Arabidopsis thaliana. Plant J 2: 103–116
- Ambrose BA, Lerner DR, Ciceri P, Padilla CM, Yanofsky MF, Schmidt RJ (2000) Molecular and genetic analyses of the silky1 gene reveal conservation in floral organ specification between eudicots and monocots. Mol Cell 5: 569–579
- Bai F, Reinheimer R, Durantini D, Kellogg EA, Schmidt RJ (2012) TCP transcription factor, BRANCH ANGLE DEFECTIVE 1 (BAD1), is required for normal tassel branch angle formation in maize. Proc Natl Acad Sci USA 109: 12225–12230
- Benlloch R, Berbel A, Serrano-Mislata A, Madueno F (2007) Floral Initiation and Inflorescence Architecture: A Comparative View. Ann Bot 100: 1609–1609
- Boden SA, Cavanagh C, Cullis BR, Ramm K, Greenwood J, Jean Finnegan E, Trevaskis B, Swain SM (2015) Ppd-1 is a key regulator of inflorescence architecture and paired spikelet development in wheat. Nat Plants 1: 14016
- Bolduc N, Yilmaz A, Mejia-Guerra MK, Morohashi K, O'Connor D, Grotewold E, Hake S (2012) Unraveling the KNOTTED1 regulatory network in maize meristems. Genes Dev 26: 1685–1690
- Bommert P, Whipple C (2018) Grass inflorescence architecture and meristem determinacy. Semin Cell Dev Biol **79**: 37–47
- Bortiri E, Chuck G, Vollbrecht E, Rocheford T, Martienssen R, Hake S (2006) ramosa2 encodes a LATERAL ORGAN BOUNDARY domain protein that determines the fate of stem cells in branch meristems of maize. Plant Cell 18: 574–585
- **Bowman JL, Alvarez J, Weigel D, Meyerowitz EM, Smyth DR** (1993) Control of flower development in *Arabidopsis thaliana* by APETALA1 and interacting genes. Development **119**: 721–743
- Bradley D, Ratcliffe O, Vincent C, Carpenter R, Coen E (1997)
 Inflorescence commitment and architecture in Arabidopsis.
 Science 275: 80–83
- Candela H, Johnston R, Gerhold A, Foster T, Hake S (2008) The milkweed pod1 gene encodes a KANADI protein that is required for abaxial/adaxial patterning in maize leaves. Plant Cell 20: 2073–2087
- Čermák T, Curtin SJ, Gil-Humanes J, Čegan R, Kono TJY, Konečná E, Belanto JJ, Starker CG, Mathre JW, Greenstein RL et al. (2017) A Multipurpose Toolkit to Enable Advanced Genome Engineering in Plants. Plant Cell 29: 1196–1217
- Chen A, Dubcovsky J (2012) Wheat TILLING mutants show that the vernalization gene VRN1 down-regulates the flowering repressor VRN2 in leaves but is not essential for flowering. PLoS Genet 8: e1003134
- Chuck G, Meeley RB, Hake S (1998) The control of maize spikelet meristem fate by theAPETALA2-like gene indeterminate spikelet1. Genes Dev 12: 1145–1154
- **Chuck G, Meeley R, Hake S** (2008) Floral meristem initiation and meristem cell fate are regulated by the maize AP2 genes ids1 and sid1. Development **135**: 3013–3019
- Chuck G, Meeley R, Irish E, Sakai H, Hake S (2007) The maize tasselseed4 microRNA controls sex determination and meristem cell fate by targeting Tasselseed6/indeterminate spikelet1. Nat Genet 39: 1517–1521
- Colasanti J, Yuan Z, Sundaresan V (1998) The indeterminate gene encodes a zinc finger protein and regulates a leaf-generated signal required for the transition to flowering in maize. Cell **93**: 593–603
- Danilevskaya ON, Meng X, Ananiev EV (2010) Concerted modification of flowering time and inflorescence architecture by ectopic expression of TFL1-like genes in maize. Plant Physiol **153**: 238–251
- Danilevskaya ON, Meng X, Hou Z, Ananiev EV, Simmons CR (2008) A genomic and expression compendium of the expanded PEBP gene family from maize. Plant Physiol 146: 250–264
- **Ditta G, Pinyopich A, Robles P, Pelaz S, Yanofsky MF** (2004) The SEP4 gene of *Arabidopsis thaliana* functions in floral organ and meristem identity. Curr Biol **14**: 1935–1940

- Dixon LE, Greenwood JR, Bencivenga S, Zhang P, Cockram J, Mellers G, Ramm K, Cavanagh C, Swain SM, Boden SA (2018) TEOSINTE BRANCHED1 regulates inflorescence architecture and development in bread wheat (*Triticum aestivum*). Plant Cell **30**: 563–581
- **Doust AN** (2017) The effect of photoperiod on flowering time, plant architecture, and biomass in setaria. *In* A Doust, X Diao, eds, Genetics and Genomics of Setaria. Springer International Publishing, Cham, Switzerland, pp 197–210
- Doust AN, Kellogg EA (2002) Inflorescence diversification in the panicoid "bristle grass" clade (Paniceae, Poaceae): evidence from molecular phylogenies and developmental morphology. Am J Bot 89: 1203–1222
- Doust AN, Mauro-Herrera M, Hodge JG, Stromski J (2017) The C4 model grass setaria is a short day plant with secondary long day genetic regulation. Front Plant Sci 8: 1062
- Endo-Higashi N, Izawa T (2011) Flowering time genes Heading date 1 and Early heading date 1 together control panicle development in rice. Plant Cell Physiol 52: 1083–1094
- Eveland AL, Goldshmidt A, Pautler M, Morohashi K, Liseron-Monfils C, Lewis MW, Kumari S, Hiraga S, Yang F, Unger-Wallace E, et al. (2014) Regulatory modules controlling maize inflorescence architecture. Genome Res 24: 431–443
- **Ferrándiz C, Gu Q, Martienssen R, Yanofsky MF** (2000) Redundant regulation of meristem identity and plant architecture by FRUITFULL, APETALA1 and CAULIFLOWER. Development **127**: 725–734
- Fornara F, Pařenicová L, Falasca G, Pelucchi N, Masiero S, Ciannamea S, Lopez-Dee Z, Altamura MM, Colombo L, Kater MM (2004) Functional characterization of OsMADS18, a member of the AP1/SQUA subfamily of MADS box genes. Plant Physiol 135: 2207–2219
- **Hodge JG, Kellogg EA** (2016) Abscission zone development in Setaria viridis and its domesticated relative, Setaria italica. Am J Bot **103**: 998–1005
- Honma T, Goto K (2001) Complexes of MADS-box proteins are sufficient to convert leaves into floral organs. Nature 409: 525–529
- Huala E, Sussex IM (1992) LEAFY interacts with floral homeotic genes to regulate Arabidopsis floral development. Plant Cell 4: 901–913
- Huang C, Sun H, Xu D, Chen Q, Liang Y, Wang X, Xu G, Tian J, Wang C, Li D, et al. (2018) ZmCCT9 enhances maize adaptation to higher latitudes. Proc Natl Acad Sci USA 115: E334–E341
- Huang P, Jiang H, Zhu C, Barry K, Jenkins J, Sandor L, Schmutz J, Box MS, Kellogg EA, Brutnell TP (2017) Sparse panicle1 is required for inflorescence development in Setaria viridis and maize. Nat Plants 3: 17054
- **Huynh-Thu VA, Irrthum A, Wehenkel L, Geurts P** (2010) Inferring regulatory networks from expression data using tree-based methods. PLoS One **5**: e12776
- Irish VF, Sussex IM (1990) Function of the apetala-1 gene during Arabidopsis floral development. Plant Cell 2: 741–753
- Jeon JS, Lee S, Jung KH, Yang WS, Yi GH, Oh BG, An G (2000) Production of transgenic rice plants showing reduced heading date and plant height by ectopic expression of rice MADS-box genes. Mol Breed 6: 581–592
- Jin J, Tian F, Yang DC, Meng YQ, Kong L, Luo J, Gao G (2017)
 PlantTFDB 4.0: toward a central hub for transcription factors and regulatory interactions in plants. Nucleic Acids Res 45: D1040–D1045
- Juarez MT, Twigg RW, Timmermans MCP (2004) Specification of adaxial cell fate during maize leaf development. Development 131: 4533–4544
- Kaneko-Suzuki M, Kurihara-Ishikawa R, Okushita-Terakawa C, Kojima C, Nagano-Fujiwara M, Ohki I, Tsuji H, Shimamoto K, Taoka KI (2018) TFL1-like proteins in rice antagonize rice FT-like protein in inflorescence development by competition for complex formation with 14-3-3 and FD. Plant Cell Physiol **59**: 458–468

- Kaufmann K, Wellmer F, Muiño JM, Ferrier T, Wuest SE, Kumar V, Serrano-Mislata A, Madueño F, Krajewski P, Meyerowitz EM, et al. (2010) Orchestration of floral initiation by APETALA1. Science 328: 85–89
- Kempin SA, Savidge B, Yanofsky MF (1995) Molecular basis of the cauliflower phenotype in Arabidopsis. Science 267: 522–525
- Kobayashi K, Maekawa M, Miyao A, Hirochika H, Kyozuka J (2010) PANICLE PHYTOMER2 (PAP2), encoding a SEPALLATA subfamily MADS-box protein, positively controls spikelet meristem identity in rice. Plant Cell Physiol 51: 47–57
- Kobayashi K, Yasuno N, Sato Y, Yoda M, Yamazaki R, Kimizu M, Yoshida H, Nagamura Y, Kyozuka J (2012) Inflorescence meristem identity in rice is specified by overlapping functions of three AP1/FUL-like MADS box genes and PAP2, a SEPALLATA MADS box gene. Plant Cell 24: 1848–1859
- Koppolu R, Anwar N, Sakuma S, Tagiri A, Lundqvist U, Pourkheirandish M, Rutten T, Seiler C, Himmelbach A, Ariyadasa R et al. (2013) Six-rowed spike4 (Vrs4) controls spikelet determinacy and row-type in barley. Proc Natl Acad Sci USA 110: 13198–13203
- Kozaki A, Hake S, Colasanti J (2004) The maize ID1 flowering time regulator is a zinc finger protein with novel DNA binding properties. Nucleic Acids Res 32: 1710–1720
- Kumar S, Stecher G, Tamura K (2016) MEGA7: molecular evolutionary genetics analysis version 7.0 for bigger datasets. Mol Biol Evol 33: 1870–1874
- Langfelder P, Horvath S (2008) WGCNA: an R package for weighted correlation network analysis. BMC Bioinformatics 9: 559
- Liang Y, Liu Q, Wang X, Huang C, Xu G, Hey S, Lin HY, Li C, Xu D, Wu L et al. (2019) ZmMADS69 functions as a flowering activator through the ZmRap2.7-ZCN8 regulatory module and contributes to maize flowering time adaptation. New Phytol 221: 2335–2347
- Li C, Lin H, Chen A, Lau M, Jernstedt J, Dubcovsky J (2019) Wheat VRN1, FUL2 and FUL3 play critical and redundant roles in spikelet development and spike determinacy. Development 146: dev175398
- Liljegren SJ, Gustafson-Brown C, Pinyopich A, Ditta GS, Yanofsky MF (1999) Interactions among APETALA1, LEAFY, and TERMINAL FLOWER1 specify meristem fate. Plant Cell 11: 1007–1018
- Li P, Brutnell TP (2011) Setaria viridis and Setaria italica, model genetic systems for the Panicoid grasses. J Exp Bot 62: 3031–3037
- Litt A, Irish VF (2003) Duplication and diversification in the APETALA1/FRUITFULL floral homeotic gene lineage: implications for the evolution of floral development. Genetics 165: 821–833
- **Liu H, Ding Y, Zhou Y, Jin W, Xie K, Chen LL** (2017) CRISPR-P 2.0: an improved CRISPR-Cas9 tool for genome editing in plants. Mol Plant **10**: 530–532
- Liu H, Song S, Xing Y (2019) Beyond heading time: FT-like genes and spike development in cereals. J Exp Bot 70: 1–3
- Lu SJ, Wei H, Wang Y, Wang HM, Yang RF, Zhang XB, Tu JM (2012) Overexpression of a transcription factor OsMADS15 modifies plant architecture and flowering time in rice (Oryza sativa L.). Plant Mol Biol Rep 30: 1461–1469
- Mamidi S, Healey A, Huang P, Grimwood J, Jenkins J, Barry K, Sreedasyam A, Shu S, Lovell JT, Feldman M et al. (2020) The Setaria viridis genome and diversity panel enables discovery of a novel domestication gene. bioRxiv 744557
- McConnell JR, Emery J, Eshed Y, Bao N, Bowman J, Barton MK (2001) Role of PHABULOSA and PHAVOLUTA in determining radial patterning in shoots. Nature **411**: 709–713
- McSteen P, Laudencia-Chingcuanco D, Colasanti J (2000) A floret by any other name: control of meristem identity in maize. Trends Plant Sci 5: 61-66
- Michelmore RW, Paran I, Kesseli RV (1991) Identification of markers linked to disease-resistance genes by bulked segregant analysis: a rapid method to detect markers in specific genomic

- regions by using segregating populations. Proc Natl Acad Sci USA 88: 9828-9832
- Nakagawa M, Shimamoto K, Kyozuka J (2002) Overexpression of RCN1 and RCN2, rice TERMINAL FLOWER 1/CENTRORADIALIS homologs, confers delay of phase transition and altered panicle morphology in rice. Plant J 29: 743–750
- Pautler M, Eveland AL, LaRue T, Yang F, Weeks R, Lunde C, Je Bl, Meeley R, Komatsu M, Vollbrecht E et al. (2015) FASCIATED EAR4 encodes a bZIP transcription factor that regulates shoot meristem size in maize. Plant Cell 27: 104–120
- Pelaz S, Ditta GS, Baumann E, Wisman E, Yanofsky MF (2000) B and C floral organ identity functions require SEPALLATA MADS-box genes. Nature 405: 200–203
- **Piñeiro M, Coupland G** (1998) The control of flowering time and floral identity in Arabidopsis. Plant Physiol **117**: 1–8
- Preston JC, Christensen A, Malcomber ST, Kellogg EA (2009) MADS-box gene expression and implications for developmental origins of the grass spikelet. Am J Bot 96: 1419–1429
- **Preston JC, Kellogg EA** (2008) Discrete developmental roles for temperate cereal grass VERNALIZATION1/FRUITFULL-like genes in flowering competency and the transition to flowering. Plant Physiol **146**: 265–276
- Preston JC, Kellogg EA (2007) Conservation and divergence of APETALA1/FRUITFULL-like gene function in grasses: evidence from gene expression analyses. Plant J 52: 69–81
- Preston JC, Kellogg EA (2006) Reconstructing the evolutionary history of paralogous APETALA1/FRUITFULL-like genes in grasses (Poaceae). Genetics 174: 421–437
- Satoh-Nagasawa N, Nagasawa N, Malcomber S, Sakai H, Jackson D (2006) A trehalose metabolic enzyme controls inflorescence architecture in maize. Nature 441: 227–230
- **Schneeberger K** (2014) Using next-generation sequencing to isolate mutant genes from forward genetic screens. Nat Rev Gen **15**: 662–676
- Schultz EA, Haughn GW (1991) LEAFY, a homeotic gene that regulates inflorescence development in Arabidopsis. Plant Cell 3: 771–781
- Schultz EA, Haughn GW (1993) Genetic analysis of the floral initiation process (FLIP) in Arabidopsis. Development 119: 745–765
- Serrano-Mislata A, Goslin K, Zheng B, Rae L, Wellmer F, Graciet E, Madueño F (2017) Regulatory interplay between LEAFY, APETALA1/CAULIFLOWER and TERMINAL FLOWER1: new insights into an old relationship. Plant Signal Behav 12: e1370164
- Shannon S, Meeks-Wagner DR (1991) A mutation in the Arabidopsis TFL1 gene affects inflorescence meristem development. Plant Cell 3: 877–892
- **Soltis DE, Chanderbali AS, Kim S, Buzgo M, Soltis PS** (2007) The ABC model and its applicability to basal angiosperms. Ann Bot **100**: 155–163
- Soneson C, Love MI, Robinson MD (2015) Differential analyses for RNA-seq: transcript-level estimates improve gene-level inferences. F1000Res 4: 1521
- Tanaka W, Pautler M, Jackson D, Hirano HY (2013) Grass meristems II: inflorescence architecture, flower development and meristem fate. Plant Cell Physiol **54**: 313–324
- **Theißen G, Saedler H** (2001) Floral quartets. Nature **409**: 469–471 **Van Eck J** (2018) The status of *Setaria viridis* transformation: Agrobacterium-mediated to floral dip. Front Plant Sci **9**: 652
- Wahl V, Ponnu J, Schlereth A, Arrivault S, Langenecker T, Franke A, Feil R, Lunn JE, Stitt M, Schmid M (2013) Regulation of flowering by trehalose-6-phosphate signaling in *Arabidopsis thaliana*. Science **339**: 704–707
- Weigel D, Alvarez J, Smyth DR, Yanofsky MF, Meyerowitz EM (1992) LEAFY controls floral meristem identity in Arabidopsis. Cell **69**: 843–859
- **Whipple CJ** (2017) Grass inflorescence architecture and evolution: the origin of novel signaling centers. New Phytologist **216**: 367–372

- Whipple CJ, Ciceri P, Padilla CM, Ambrose BA, Bandong SL, Schmidt RJ (2004) Conservation of B-class floral homeotic gene function between maize and Arabidopsis. Development 131: 6083–6091
- Whipple CJ, Zanis MJ, Kellogg EA, Schmidt RJ (2007) Conservation of B class gene expression in the second whorl of a basal grass and outgroups links the origin of lodicules and petals. Proc Natl Acad Sci USA 104: 1081–1086
- Wimalanathan K, Lawrence-Dill CJ (2019) Gene ontology meta annotator for plants. bioRxiv 809988; doi: 10.1101/809988
- Wu D, Liang W, Zhu W, Chen M, Ferrándiz C, Burton RA, Dreni L, Zhang D (2018) Loss of LOFSEP transcription factor function converts spikelet to leaf-like structures in rice. Plant Physiol 176: 1646–1664
- Wu F, Shi X, Lin X, Liu Y, Chong K, Theißen G, Meng Z (2017)
 The ABCs of flower development: mutational analysis of AP1/FUL-like genes in rice provides evidence for a homeotic (A)-function in grasses. Plant J 89: 310–324
- Wu J, Lawit SJ, Weers B, Sun J, Mongar N, Van Hemert J, Melo R, Meng X, Rupe M, Clapp J et al. (2019) Overexpression of zmm28 increases maize grain yield in the field. Proc Natl Acad Sci USA 116: 23850–23858
- Yang J, Thames S, Best NB, Jiang H, Huang P, Dilkes BP, Eveland AL (2018) Brassinosteroids modulate meristem fate and

- differentiation of unique inflorescence morphology in Setaria viridis. Plant Cell **30**: 48–66
- Yan L, Loukoianov A, Tranquilli G, Helguera M, Fahima T, Dubcovsky J (2003) Positional cloning of the wheat vernalization gene VRN1. Proc Natl Acad Sci USA 100: 6263–6268
- Yu G, Wang LG, Han Y, He QY (2012) cluster Profiler: an R package for comparing biological themes among gene clusters. OMICS 16: 284–287
- Zhang L, Li Q, Dong H, He Q, Liang L, Tan C, Han Z, Yao W, Li G, Zhao H et al. (2015) Three CCT domain-containing genes were identified to regulate heading date by candidate genebased association mapping and transformation in rice. Sci Rep 5: 7663
- Zhou F, Lin Q, Zhu L, Ren Y, Zhou K, Shabek N, Wu F, Mao H, Dong W, Gan L et al. (2013) D14–SCF D3-dependent degradation of D53 regulates strigolactone signalling. Nature **504**: 406–410
- Zhu C, Yang J, Box MS, Kellogg EA, Eveland AL (2018) A dynamic co-expression map of early inflorescence development in Setaria viridis provides a resource for gene discovery and comparative genomics. Front Plant Sci 9: 1309
- Zou LP, Sun XH, Zhang ZG, Liu P, Wu JX, Tian CJ, Qiu JL, Lu TG (2011) Leaf rolling controlled by the homeodomain leucine zipper class IV gene Roc5 in rice. Plant Physiol 156: 1589–1602